AN ANALYSIS OF NONLINEAR ELASTIC DEFORMATIONS FOR A HOMOGENEOUS BEAM AT VARYING TIP LOADS AND PITCH ANGLES

THESIS

Robert J. McGraw, Ensign, USN

AFIT/GAE/ENY/06-J09

DEPARTMENT OF THE AIR FORCE
AIR UNIVERSITY

AIR FORCE INSTITUTE OF TECHNOLOGY

Wright-Patterson Air Force Base, Ohio

The views expressed in this thesis are those of the author and do not reflect the official policy or position of the United States Air Force, the United States Navy, Department of Defense, or the U.S. Government.

AFIT/GAE/ENY/06-J09

AN ANALYSIS OF NONLINEAR ELASTIC DEFORMATIONS FOR A HOMOGENEOUS BEAM AT VARYING TIP LOADS AND PITCH ANGLES

THESIS

Presented to the Faculty

Department of Aeronautics and Astronautics

Graduate School of Engineering and Management

Air Force Institute of Technology

Air University

Air Education and Training Command

In Partial Fulfillment of the Requirements for the

Degree of Master of Science in Aeronautical Engineering

Robert J. McGraw, BS

Ensign, USN

June 2006

AFIT/GAE/ENY/06-J09

AN ANALYSIS OF NONLINEAR ELASTIC DEFORMATIONS FOR A HOMOGENEOUS BEAM AT VARYING TIP LOADS AND PITCH ANGLES

Robert J. McGraw, BS

Ensign, USN

Approved:

Dr. Donald L. Kunz (Chairman)	Date
Dr. Robert A. Canfield (Member)	Date
Maj. Eric D. Swenson (Member)	Date

Abstract

The Princeton beam experiments of 1975 were performed in hopes of producing viable data for beam nonlinear elastic deformation models in hopes of improving helicopter main beam designs. The recorded data, specifically for homogeneous beams of 7075 aluminum, have been referenced as a baseline for the past thirty years to validate numerous computer models and theories in an effort to build beams capable of withstanding aeroelastic, static, and dynamic loading.

The purpose of this study is to improve upon the data recorded in 1975 using newer technologies including a laser distance meter, digital inclinometer, and three-dimensional traverse to test X-axis, Y-axis, Z-axis and angular displacements for varying tip loads and pitch angles.

Initial beam deformations due to machining stresses were included in the testing, and the beam was analyzed at tip loads between zero and four pounds for positive and negative pitch angles in fifteen-degree increments from zero to ninety degrees. The results were analyzed in numerous comparisons between the different tip loads and pitch angles, and the overall results were compared with Princeton beam data to ensure their validity.

The experimental results showed an improvement in terms of precision as well as a relatively close correlation with Princeton beam data. There were some displacement discrepancies, but such differences can be examined in the future. The results can be used for beam vibrational mode and frequency testing as the beam's geometry can be reproduced graphically and computer model verifications, allowing for more precise computer models for homogeneous nonlinear beam displacements.

In memory of my Grandfather, friend and veteran.

Acknowledgments

This report is submitted with deepest gratitude to Dr. Kunz (advisor), Maj. Swenson and Dr. Canfield (readers), Mr. Wilbur Lacy, and Mr. Jay Anderson. I appreciate all of your help, and I will think of you fondly when I have moved to Florida and realized my dream of leaving Ohio.

Table of Contents

Abstract iv

Acknowledgments vi

Table of Contents vii

List of Figures ix

List of Tables xi

1. Introduction 1

    1.1 The Princeton Beam Experiments 1

    1.2 Purpose 1

    1.3 Methodology 2

    1.4 Assumptions 4

    1.5 Implications 4

2. Literature Review 1

    2.1 The Princeton Beam Experiments 1

    2.2 Princeton Beam References 4

        2.2.1 Rotorcraft Dynamics Division (1987) 5

        2.2.2 Hinnant and Hodges (1988) 5

        2.2.3 Hopkins and Ormiston (2003) 6

        2.2.4 Hodges (2005) 7

3. Methodology 8

    3.1 Experimental Components 8

        3.1.1 Traverse 8

        3.1.2 Control/Driver 9

        3.1.3 Inclinometer 10

        3.1.4 Laser Distance Meter 10

        3.1.5 Multimeter 12

        3.1.6 Main Beam 13

        3.1.7 Static Loading Weights 13

        3.1.8 Swiveling Hub 14

3.2 Setup 14
3.2.1 Laser Distance Meter/Traverse 14
3.2.2 Beam Preparation 15
3.2.3 Base Column/Swiveling Hub 15
3.2.4 Hanging Weights 15
3.3 Procedure 16
3.3.1 Initial Testing 17
3.3.2 Procedural Improvements 20
3.3.3 Revised Procedure 21
4. Results and Analysis 25
4.1 Deflection Analyses 25
4.1.1 X Axis Deflection 25
4.1.2 Z Axis Deflection 29
4.1.3 Angular Deflection 34
4.1.4 Tip Load Comparisons 36
4.2 Comparison with Princeton Beam Data 39
4.3 General Analyses 43
4.4 Linear v Nonlinear 45
4.5 Measurement Errors 46
5. Summary 48
5.1 Future Improvements 48
5.2 Implications 50
5.3 Conclusions 50
Appendix A: Corrected Data 52
Appendix B: Original Data 66
Appendix C: Princeton Beam Data 79
6. Works Cited 88

List of Figures

Figure 1: General notation 1
Figure 2: Side-view of Beam #2 3
Figure 3: X-Z axis system 3
Figure 4: Traverse 9
Figure 5: NCDT placement 12
Figure 6: Multimeter display 13
Figure 7: Experimental setup 16
Figure 8: Data point locations 19
Figure 9: NCDT angular disadvantage 22
Figure 10: X Deflection (0 deg) 26
Figure 11: X Deflection (30 deg) 26
Figure 12: X Deflection (-30 deg) 27
Figure 13: X Deflection (60 deg) 28
Figure 14: X Deflection (-60 deg) 28
Figure 15: X Deflection (90 deg) 29
Figure 16: Z Deflection (0 deg) 30
Figure 17: Z Deflection (30 deg) 31
Figure 18: Z Deflection (-30 deg) 31
Figure 19: Z Deflection (60 deg) 32
Figure 20: Z Deflection (-60 deg) 32
Figure 21: Z Deflection (90 deg) 33
Figure 22: Angular Deflection (30 deg) 34
Figure 23: Angular Deflection (60 deg) 35
Figure 24: Angular Deflection (90 deg) 35
Figure 25: Tip Load v Tip X Deflection 36
Figure 26: Tip Load v Tip Y Deflection 37
Figure 27: Tip Load v Tip Z Deflection 38
Figure 28: Tip Load v Tip Pitch Angle Deflection 38
Figure 29: X Comparison of +/- 30 deg trials 40

Figure 30: X Comparison of +/- 60 deg trials 40
Figure 31: Z Comparison of +/-30 deg trials 41
Figure 32: Z Comparison of +/-60 deg trials 42
Figure 33: Angular Comparison of +/- 30 deg trials 42
Figure 34: Angular Comparison of +/- 60 deg trials 43
Figure 35: Linear v nonlinear (90 deg) 45

List of Tables

Table 1: Current v Princeton precision 47
Table 2: Weight nomenclature 52
Table 3: Corrected Data (0 deg) 53
Table 4: Corrected Data (15 deg) 54
Table 5: Corrected Data (-15 deg) 55
Table 6: Corrected Data (30 deg) 56
Table 7: Corrected Data (-30 deg) 57
Table 8: Corrected Data (45 deg) 58
Table 9: Corrected Data (-45 deg) 59
Table 10: Corrected Data (60 deg) 60
Table 11: Corrected Data (-60 deg) 61
Table 12: Corrected Data (75 deg) 62
Table 13: Corrected Data (-75 deg) 63
Table 14: Corrected Data (90 deg) 64
Table 15: Corrected Data (-90 deg) 65
Table 16: Corrected Data (180 deg) 65
Table 17: Original Data (0 deg) 66
Table 18: Original Data (15 deg) 67
Table 19: Original Data (-15 deg) 68
Table 20: Original Data (30 deg) 69
Table 21: Original Data (-30 deg) 70
Table 22: Original Data (45 deg) 71
Table 23: Original Data (-45 deg) 72
Table 24: Original Data (60 deg) 73
Table 25: Original Data (-60 deg) 74
Table 26: Original Data (75 deg) 75
Table 27: Original Data (-75 deg) 76
Table 28: Original Data (90 deg) 77
Table 29: Original Data (-90 deg) 78

Table 30: Original Data (180 deg) 78
Table 31: Princeton data (0 deg) 79
Table 32: Princeton data (15 deg) 80
Table 33: Princeton data (-15 deg) 81
Table 34: Princeton data (30 deg) 82
Table 35: Princeton data (-30 deg) 83
Table 36: Princeton data (45 deg) 83
Table 37: Princeton data (-45 deg) 84
Table 38: Princeton data (60 deg) 84
Table 39: Princeton data (-60 deg) 85
Table 40: Princeton data (75 deg) 85
Table 41: Princeton data (-75 deg) 86
Table 42: Princeton data (90 deg) 86
Table 43: Princeton data (-90 deg) 87
Table 44: Princeton data (180 deg) 87

AN ANALYSIS OF NONLINEAR ELASTIC DEFORMATIONS FOR A HOMOGENEOUS BEAM AT VARYING TIP LOADS AND PITCH ANGLES

1. Introduction

1.1 The Princeton Beam Experiments

Performed in two separate installments in 1975, Dowell and Traybar's Princeton beam experiments have served as a basis for helicopter main beam elastic nonlinear deformation models regarding homogeneous blades at varying pitch angles and static tip loads. The experiments examined the vibrational modes and static deformations of three different beams of 7075 aluminum, all with differing dimensions. The experiments have been used for over thirty years as a benchmark for homogeneous beam deflection models. Their data has been used to validate analytical models as recently as 2003 and 2005 by Hopkins and Ormiston, and Hodges, respectively. The beam experiments implemented unavoidable mechanical errors, mostly due to the displacement and vibrational equipment available in the mid-1970s. Dowell and Traybar's initial experiment left room for improvement, as they assumed the beam to be perfectly straight at tip loads of zero pounds, though it was reportedly deformed prior to static loading. The availability of contact-free displacement measurement devices, digital angular measurements, and various other modern techniques can be applied to improve Princeton beam data, thus formulating a set of results to which computer models may be more accurately compared.

1.2 Purpose

The purpose of this technical report is to reproduce the Princeton beam experiments with improvements in equipment, experimental procedures, initial

assumptions, and more sensitive displacement readouts in hopes of forming a more precise set of test data to which one may compare nonlinear elastic deformation models for homogeneous beams. The beam's initial deformations, due to machining stresses, will be taken in to account throughout testing, and the experiment will be improved overall in terms of precision and methodology.

1.3 Methodology

For purposes of improving over past data, the beam deformation displacement measurements were taken using more modern equipment to include a digital inclinometer for angle measurements, a three-dimensional traverse, a no-contact laser distance meter for displacement measurements, a digital multimeter, and an apparatus designed to secure the beam at different pitch angles for load testing. The digital inclinometer will be employed to acquire reliable beam root pitch angles. The inclinometer was attached to a swiveling hub/base column setup to which the beam was bolted to the optics table. As the hub and beam turned in unison, so did the inclinometer, providing a digital readout of the beam position with respect to the vertical axis.

The traverse was outfitted with a laser distance meter (optoNCDT) that was "normalized" to the designated origin at the root of the beam. Using the laser to locate the positions at which data was taken, the multimeter provided a measurement of the NCDT's distance from the top of the beam in terms of voltage. The NCDT was designed to bounce a wavelength of light against a given target and receive the returning signal to provide displacement measurements through laser triangulation. The traverse was controlled via a Velmex Control/Driver that operated its three individual motors, one on each of the coordinate axes. The controller produced displacement readouts precise to

hundredths of a millimeter by monitoring the traverse's motor revolutions in relation to the threads on each traverse axis.

As in the Princeton beam experiments, the beam was tested at positive and negative pitch angles from zero to ninety degrees in fifteen-degree increments. To allow for a complete data set, the beam was also tested at 180º. For individual trials, the weights was loaded on the beam in increasing amounts, between zero and four pounds, as the traverse maneuvered up and down the length of the beam, or its Y-axis, and the control/driver provided data points at a rate of two for each of the five spanwise stations. The laser's visible output was used to pinpoint exact locations at the spanwise stations, and the multimeter's readouts were maintained at a specified voltage. This ensured that the NCDT was the same distance from the beam at every point, and the displacements along the Z-axis were noted via the controller's output. As coordinates for both points were recorded for the final spanwise station, the beam was reloaded with a higher weight, and data was recorded and the traverse was returned to the hub/base column arrangement. In this manner, the displacements for the beam at all given angles and tip loads were produced with precision in a less time-consuming method.

Following data collection, the coordinates for each of the spanwise stations were reproduced in terms of the beam's elastic axis and then incorporated into numerous figures, tables, and charts to provide visual representations of initial pitch angle and static tip load correlations. The angular displacements at each spanwise station were calculated using the X- and Z-axis displacement coordinates and the arctangent function for twist angle. The measurements were tabulated and reported for each of the trials.

1.4 Assumptions

A few assumptions were made throughout the course of the project to ensure the data was recorded accurately and efficiently. The beam was assumed to have initial deformations from machining stresses, and it was tested with a tip load of zero pounds at every initial pitch angle. The weights were measured to within 0.01lb, and any values on chart and figures were assumed to contain an error of plus or minus 0.01lb. The swiveling hub, beam, and base column apparatus were all carefully assembled to produce perpendicular angles with reference to the optics table and the three-dimensional traverse. The set-up was assumed to maintain consistent perpendicularity, meaning the beam was projected directly parallel to the Y-axis of the traverse. The traverse was assumed to have no internal malfunctions pertaining to its threading or motorized axes. The traverse's original location was checked regularly during testing, but the traverse was considered to be mechanically sound to produce viable results. The NCDT as well was considered mechanically and electronically sound, as its displacement measurements were the major component of Z-axis deflection data. The air temperature was assumed to remain at 75^{o}F, so that all normal mechanical properties for 7075 aluminum applied.

1.5 Implications

The Princeton beam experiments were referenced for comparison purposes for numerous nonlinear beam deformation models, and the improvement of said experiments only serves to improve future computer codes for rotorcraft mechanics and dynamics. The data presented here were by no means perfect, but the goal was to gain a better understanding of the experimental correlations between static tip loads and their respective deformations at varying pitch angles.

2. Literature Review

2.1 The Princeton Beam Experiments

Conducted in January of 1975 by E.H. Dowell and J.J. Traybar in preparation for the U.S. Air Mobility and Research Development Laboratory, the Princeton Beam Experiments were a study of the flap, lag, and twist associated with nonlinear deformations of a 7075 aluminum beam. The general idea was to determine the effect of point loads on a helicopter beam by testing its static deflection and vibrational modes at different pitch angles between 0º and 180º and compare that data with a nonlinear deformation model produced by Hodges and Dowell. Dowell and Traybar's axis and angular systems are reproduced in Figure 1. The pitch angle was measured from the vertical axis to the beam's root or tip, using nothing more than rulers and graph paper.

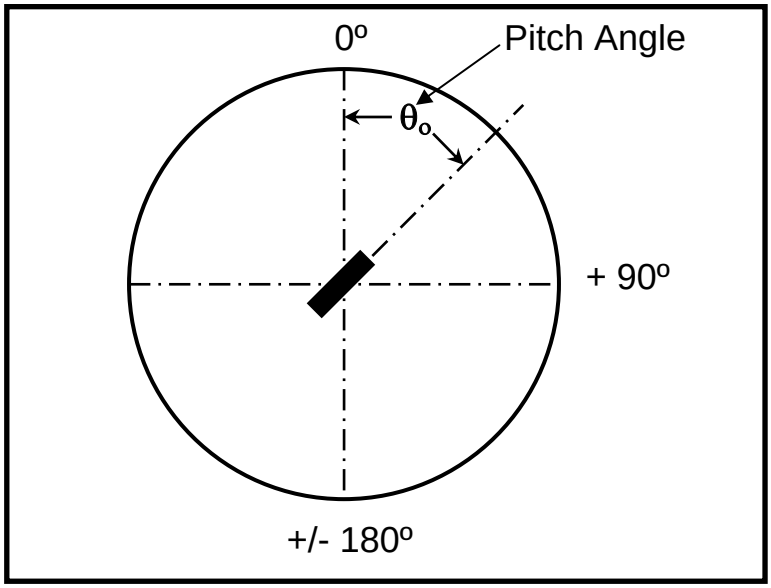

Figure 1: General notation

A designated pitch angle was determined for the root of the beam, while the absolute value of its tip pitch angle increased with increasing loads. This representation shows

only the tip deflection of a given beam with no regard to its deflection along the horizontal axis.

Entitled “An Experimental Study of the Nonlinear Stiffness of a Beam Undergoing Flap, Lag, and Twist Deformations,” the report considered three different beams of varying dimensions. The three beams tested were $20*1*1/8in^3$ (Beam #1), $20*1/2*1/8in^3$ (Beam #2), and $30*1/2*1/8in^3$ (Beam #3). The tips of each beam were loaded with weights from zero to five pounds in magnitude and then tested to determine vibrational modes, static deflections (on the vertical axis), and angular variations from the root of the beam to the tip. Beam #s 1 and 2 were used for static deflection testing, while Beam #s 2 and 3 were used for vibrational mode testing. The data was relatively scattered, thus promoting additional testing in December of 1975.

Dowell and Traybar’s addendum to their initial experiments incorporated a new set of static deflection testing data for Beam #2. Using body-fixed axes (X and Z) and converting to space-fixed axes (W and V), the report provided more accurate data for nonlinear static deformations than the original experiments produced in January of that year. Instead of measuring static deflection and pitch angle with graph paper and rulers, a dialtype caliper measuring scale (precise to three or four decimal places) was mounted to a flat table to test the initial curvature of the beam and its subsequent deflections when loaded. The curvature was minor, probably due to internal machining stresses. As the beam deflected with increasing loads, Dowell and Traybar used a flat-table configuration to measure its movement in the X direction utilizing a grid on the table itself. To measure movement in the Z direction, sharpened aluminum rods were placed on the flat-table configuration and traversed to pinpoint the exact locations to which the beam deflected.

For Beam #2, a measurement of X and Z displacement was taken every five inches with the root assumed to be its origin, thus creating four data points for each different trial (Figure 2). Using their new methods, they increased precision from 0.1in to 0.001in for

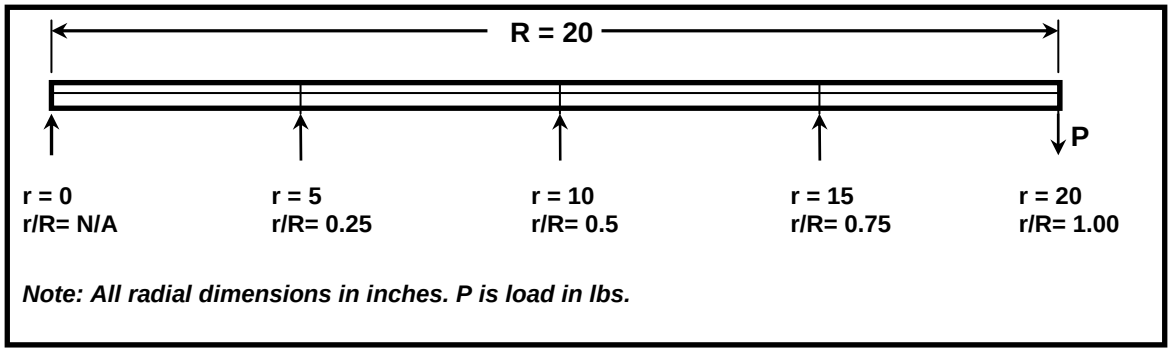

Figure 2: Side-view of Beam #2

vertical displacement and 0.1in to 0.01in for horizontal displacement. 1975's data was more precise in comparison to Hodges and Dowell's nonlinear deformation models. The body-fixed axis system is noted in Figure 3 from a view of the beam's tip.

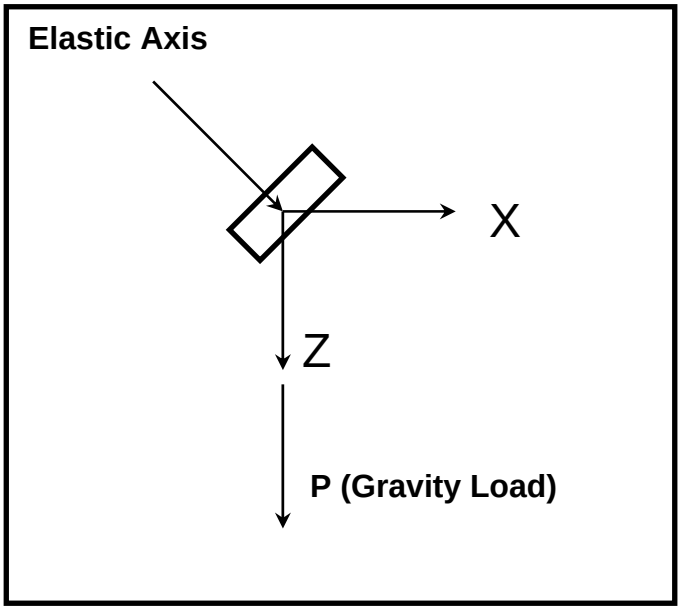

Figure 3: X-Z axis system

The Princeton beam experiments were performed assuming a straight beam with no initial important deformations. Hence, the beam was measured for different tip loads

and angles, but at tip loads of zero pounds, the elastic axis was assumed to have zero displacement in all directions. By examining Hopkins and Ormiston's introductions and procedures for both the original experiments and the addendum, Hopkins and Ormiston actually noted that the beam did have initial deformations. The two experimenters referenced it prior to testing but never accounted for the deformations in actual data tables or presented figures.

The Princeton beam experiment's data were recorded using experimental procedures that were available at the time. The methods were not as precise as they could have been, so Hopkins and Ormiston produced a certain amount of human error as all experiments do. Flat-table configurations, aluminum rods connected along the width of the beam for angular displacement measurements, and a human-produced grid resulted in various discrepancies, providing less than precise results that did not match Hodges and Dowell's model at higher static loads. The experiments were, however, accepted and referenced in journals following December of 1975. There was room for precision improvements, but the specific technologies required for that improvement were not yet available. (Dowell)

2.2 Princeton Beam References

The Princeton Beam Experiments provided data to which many other beam deformation analyses were compared. As recently as 2003 and 2005, the 1975 results were referenced as a viable source of data for the nonlinear elastic deformation of rotorcraft blades at varying pitch angles and static loads. In May of 2003, A. Stewart Hopkins and Robert A. Ormiston presented a newly-developed model for rotorcraft blade analysis that incorporated both rigid and flexible body kinematics. Stewart and Ormiston

reported the model's results in comparison with Princeton beam data to verify their findings. In October of 2005, Dewey H. Hodges, of the Princeton beam experiment's theoretical model fame, presented his findings for three-dimensional nonhomogenous beams which were not considered with the homogenous beams of 7075 aluminum in 1975. Similar papers were presented between that year and the present, all with respect to the findings from 1975, which did not necessarily incorporate all the actual beam deformations due to some initial assumptions regarding beam warping.

2.2.1 Rotorcraft Dynamics Division (1987)

In 1987, Hodges, Hopkins, Kunz, and Hinnant of the U.S. Army's Aeroflightdynamics Directorate Rotorcraft Dynamics Division presented the General Rotorcraft Aeromechanical Stability Program (GRASP) which was designed to analyze beam aeroelastic, static, and dynamic deflections in its loaded and unloaded states. GRASP outputs for edgewise, torsional, and flatwise deflections at varying load angles were compared directly with Princeton beam data. The experimental and GRASP correlations were in agreement, as the program produced numbers similar to those recorded for 7075 aluminum in 1975. The average displacement error was found to be approximately 0.5%. The Princeton beam experiments were directly referenced to validate GRASP's computed outputs, much as they were referenced again only a year later. (Hodges and Hopkins)

2.2.2 Hinnant and Hodges (1988)

Following GRASP's production in 1987, Hinnant and Hodges continued the work with another report entitled "Nonlinear Analysis of a Cantilever Beam." The paper again

compared GRASP data to Princeton beam data, furthering the analyses from a year earlier by performing more testing and data comparisons. Again, the Princeton beam data served to validate GRASP outputs in a more detailed analysis, and the correlations were found to be as close as those in 1987. (Hinnant)

2.2.3 Hopkins and Ormiston (2003)

In "An Examination of Selected Problems in Beam Structural Mechanics and Dynamics," Hopkins and Ormiston produced the Rotorcraft Comprehensive Analysis System (RCAS), a computer model designed to predict beam deflections based on the types of materials used for a specific helicopter design, pitch angles for the blade, and different loads as well. The study, presented on May 6-8, 2003, to the American Helicopter Society 59th Annual Forum, outlined a comparison between the newly developed RCAS, UH-60 flight test data, Maryland vacuum chamber experiments, and the Princeton beam experimental data to determine the validity of their model. Hopkins and Ormiston designed RCAS to combine both rigid and flexible body kinematics, making the program more useful for beam deflection analyses. Hopkins and Ormiston were, however, faced with the two important tasks of verifying that the changes were correct in the model and that the combination of rigid and flexible kinematics, for nonhomogenous beams, actually showed a precision improvement over past data.

The Princeton beam experiments' nonlinear torsion results addressed an important aspect of beam nonlinear deflections. The "aeroelastic consequences" for such deformations was of great concern for beam design, and Hopkins and Ormiston directly referenced Dowell and Traybar's findings to verify the RCAS model. It was noted, in 2003, that the Princeton beam experiments were referenced numerous times in the past,

often with unsatisfactory results due to discrepancies between theoretical calculations and experimental data. The analytical solutions produced with RCAS showed these errors as well, mostly dealing with larger loads and torsional deflections. (Hopkins)

2.2.4 Hodges (2005)

In October of 2005, Dewey H. Hodges presented his paper entitled “Beams and Beam Theory: Past, Present, and Future” in which he referenced the beam experiments to add validity to his models for “static deflection under specified loading. Hodges’ purpose was to produce modern beam theory that could precisely and accurately assess a beam’s axial stresses and strains in its deformed and undeformed states. The theory, unlike Princeton beam data, was designed to produce results for varying geometries and material qualities, but Princeton data was used for comparison purposes. Such models allowed engineers to formulate blade designs with failure due to buckling loads, natural vibrations, and static and dynamic deformations in mind. (Hodges)

3. Methodology

The Princeton beam experimental measurements were accurate to 0.01in and 0.001in, but the setup included less precise methods than are currently available. Stiff rods attached perpendicularly to the beam's width and flat-table configurations were employed to measure angular deflections and beam tip displacements, as displacement were measured using basic rulers. Such a setup left much room for error, so newer technologies were incorporated to produce more viable data for future reference. The problem regarding displacement measurements produced less precise results than were later possible.

Experimental data were produced using an apparatus incorporating a laser distance meter, a traverse, a voltmeter, and an inclinometer simultaneously. The experimental apparatus was employed to test all of the beam loads at each given pitch angle, and the displacements were recorded in millimeters.

3.1 Experimental Components

3.1.1 Traverse

A basic three-dimensional Velmex traverse was acquired from AFIT's laboratory equipment storage. It was determined that, to produce beam deflection data for all three axes, an accurate, mechanical process must be incorporated in the experiment to position a laser distance meter over appropriate locations on the beam. The traverse, moving along all three axes, provided the necessary range of motion for data collection. The current displacements were measured for various tip angles and loads at spanwise stations on the beam.

Figure 4: Traverse

3.1.2 Control/Driver

A Velmex, Inc. 8300 Series Control/Driver was used along with the three-dimensional traverse. The driver served to control the traverse manually via three motors (one for each axis of the traverse). Motor numbers one, two, and three were connected to the Y-, X-, and Z-axes, respectively, and each motor controlled the traverse at four different speeds. The control/driver produced a digital readout of distance traveled in hundredths of a millimeter, and each motor could move the traverse as precisely as one hundredth of a millimeter. In addition to its added precision, the control/driver could be "zeroed," regardless of the locations of each traverse axis. Basically, this allowed the experimenter to find a location on the beam at which an origin could be established, zero the control/driver, and take data points in relation to a newly established origin. The more precise device allowed the experimenter a chance to produce more viable data than a hand-held ruler would allow.

3.1.3 Inclinometer

The SPI Protracto Level II Inclinometer measured a given incline, precise to a tenth of a degree. The inclinometer's main disadvantage was its range of only positive or negative fifty degrees, but the inclinometer could be attached to different perpendicular planes to remedy the situation. The increased precision was a grand improvement over the basic protractors and rulers used during the Princeton Beam Experiments to determine beam initial pitch angles. The inclinometer was fixed to the swiveling hub at perpendicular angles to provide a plausible pitch angle prior to each experimental trial.

3.1.4 Laser Distance Meter

In order to locate each point on the aluminum specimen accurately, a laser distance meter was employed. The Micro-Epsilon optoNCDT 1800 was designed for laser-optical displacement measurements on numerous surfaces at all angles. The optoelectronic displacement measurement system allowed for data collection with literally no interaction between the experimenter and the test specimen. Instead of recording displacements with stiff rods attached to the beam (considered negligible in the Princeton Beam Experiments), the NCDT diode projected a visible spot of light onto a given target surface. The laser then bounced back to an optical receiver, also located on the NCDT with the diode, where the spot was imaged on a CCD array, a process known as laser triangulation. Given a certain distance from a target, a laser left the NCDT's diode vertically, and when it returned at an angle to the CCD imaging array, the angle with which it met the sensor was calculated. This angle was used to calculate the

distance between the diode and CCD array was a given. All displacements were then reproduced digitally in terms of voltage. The laser triangulation occurred at a frequency of 5 kHz, making it extremely adaptable to changing surface types or distances.

Of Micro-Epsilon's numerous models, the 1800 provided the smallest allowable displacement. The NCDT could only measure its distance from the deformed beam within a range of about five centimeters, as focusing on a target too close or too far away would return the diode's laser fore or aft of the CCD imaging array, respectively. So, to gather data, the NCDT was kept at a distance that produced readouts of 1.00000 +/- 0.00050 V. This appeared to be the most "focused" range for the laser distance meter, and the meter was kept at the same distance from the beam for every displacement measurement while the control/driver produced vertical displacements via the traverse's motors.

In essence, the optoNCDT 1800 was the most viable method of data collection available. Not only did the experimenter gain information without contacting the test specimen during trials, but the visible spectrum emitted allowed each point on the beam to be targeted correctly. The diameter of the projected laser beam appeared to average around one-half of a millimeter when the NCDT was properly focused on the beam.

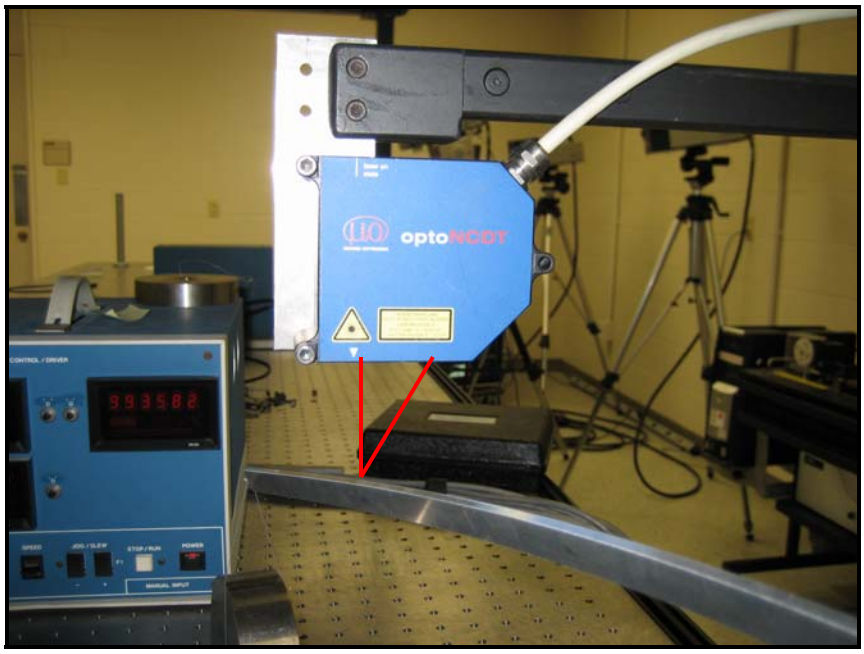

Figure 5: NCDT placement

3.1.5 Multimeter

To monitor output voltage information from Micro-Epsilon's NCDT, a Hewlett Packard Multimeter was used to receive and display the laser distance meter's displacements. Precise to a ten-thousandth of a volt, the multimeter provided a method by which the laser's distance from the beam could be determined. Using two known distances and their respective voltage readouts, the laser/multimeter combination was found to produce distance measurements of 0.01mm per 0.004 mV.

Figure 6: Multimeter display

3.1.6 Main Beam

The theoretically homogeneous beam was produced, as in the Princeton beam experiments, from a sheet of 7075 aluminum measuring an eighth of an inch thick. The beam was machined to the specifications for Beam #2, or 23in*1/2in*1/8in. The machining process caused the aluminum it to warp along its Y-axis, inducing a slight curvature that was accounted for during every experimental trial. A small hole was drilled into the beam's elastic axis (on its tip) and tapped for a machine screw diameter of 1/16in. The screw, measuring a half inch in length, was turned into the tip of the beam and considered negligible mass for the duration for the experiment.

3.1.7 Static Loading Weights

Steel weights between zero and five pounds (in half increments) were machined for vibrational beam testing, a different aspect of the Princeton beam experiments. The weights were weighted to within a hundredth of a pound (see Appendix A, Table 2), making the weights extremely precise for vibrational testing. The weights were,

however, used for static loading on the beam's tip, as the weights already contained the necessary masses for testing. Thus, the weights required for a reproduction of the former static loading experiments were conveniently available.

3.1.8 Swiveling Hub

A "swiveling hub" arrangement, onto which the aluminum beam could be perpendicularly fastened, was constructed. The hub securely bolted down the first three inches of the beam, leaving the remaining twenty inches for testing. This was required to ensure a solid base for the beam while its tip underwent nonlinear elastic deformation on all three axes.

3.2 Setup

3.2.1 Laser Distance Meter/Traverse

To accurately acquire data using the aforementioned experimental equipment, an overall setup was constructed. The three dimensional Velmex traverse was positioned perpendicularly to an optics table for testing. The laser distance meter was then attached to the traverse's data collection arm via drilled aluminum plating and basic nuts and bolts. The arm, extending horizontally from the Z-axis of the traverse to a designated data collection area, was the connection between the traverse and the NCDT. The NCDT was "aimed" in the positive Z direction, or vertically down from the traverse's arm, allowing data points to be taken from the top of the beam when statically loaded. The distance meter was then wired to the voltmeter to produce voltage readouts for distance measurements. The traverse, however, was attached to the Velmex Control/Driver, which produced digital readouts of displacement along all three axes during testing.

3.2.2 Beam Preparation

Both sides of the 7075 aluminum beam were marked at five-inch increments (starting at the tip of the beam) with a machine-working scribe. Every five inches, a mark was scribed to designate locations for data collection. Four marks were made, so a total of twenty inches were covered on either side of the blade. The last three inches were left unmarked, as they were later clamped inside the swiveling hub on the base testing apparatus.

3.2.3 Base Column/Swiveling Hub

The optical table was outfitted with a base testing apparatus, designed to support the beam horizontally on a swiveling fixture. The base column was bolted to the optics table, and the swiveling hub was bolted to the top of the base column. To the swiveling hub, the aluminum beam was secured using a bolted, flat steel plate which held the beam flush against the swiveling hub, perpendicular to the base column. The inclinometer was then attached to the swiveling hub as well, effectively attaching it to the beam itself. This gave the experimenter the ability to move the entire arrangement in unison, directly relating the inclinometer's measurements to the beam's pitch angles.

3.2.4 Hanging Weights

The hanging weights were originally machined in circular patterns to form cylinders that would fit around the tip of the beam. The vibrational testing required tip loading with weights that would result in ease of inertial moment calculations, and so the unorthodox weights were formed from steel using a lathe. However, when performing static beam testing, the weights only needed to be precise. Thus, the weights were hung

from the tip of the beam using ten-pound-test fishing line, a negligible mass considering the weight of the aluminum beam and weights to which it was attached. The weights were hung at least two inches below the tip of the beam during every trial in order to remedy any interference the weight would have induced on the laser during beam tip displacement measurements.

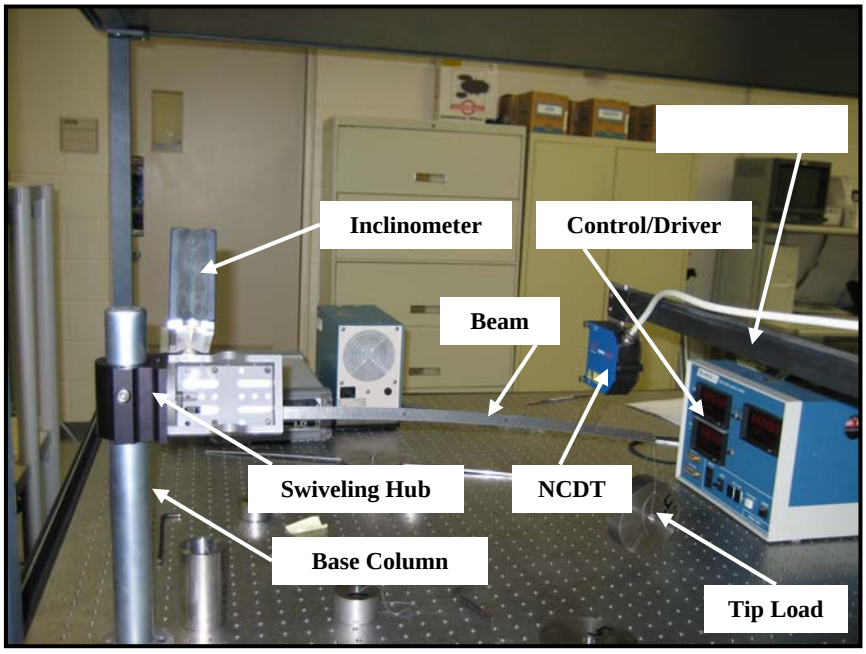

Figure 7: Experimental setup

3.3 Procedure

The procedures for testing were refined from an initial trial run involving a few different specimens to a finely-tuned method in which speed of data collection and accuracy were optimized. The data was all collected manually, so each point taken required a centering of the NCDT output on each point, located on the edges of the beam (five inches apart each, lengthwise). The traverse, working on all three axes, had to be positioned according to its Y-axis first and then moved along the X-axis to a point at which the laser contacted the beam. When the point in question was located with the

laser, the NCDT's height was controlled using the traverse's Z-axis, the voltage readout indicating how far from the top of the beam the NCDT was positioned.

Each point along the beam was placed on what was deemed a "radial station." A point's radial station was nothing more than its ratio of r/R where "R" was the entire length of the beam, or major beam radius, and "r" was the intermediate length from the hub to a given point, or minor beam radius. Each radial station was scribed as previously noted, creating two different locations for data collection at each radial station. The purpose for taking two data points at each station was to solve the Princeton beam experiments' main problem of producing viable angular deflection data. Using the width of the beam and X- and Z-axis measurements between points along the width, a simple geometric calculation would easily produce the angular measurements required.

All data was gathered from the Velmex Control/Driver in hundredths of a millimeter and recorded using Microsoft Excel. The procedure for precisely locating each point on the beam was iterative, as changing the X-, Y-, or Z-axes with the traverse often affected the positions of the laser with respect to the beam's axes.

3.3.1 Initial Testing

All data collection and testing were performed using the same spatially-fixed axes and angular assumptions as the Princeton beam experiments. From a tip view of the beam, the vertical, or Z-, axis represented a pitch angle of zero degrees, with positive and negative pitch angles clockwise and counterclockwise of the vertical, respectively.

The first trial involved a pitch angle of thirty degrees with a load of two pounds. The weight was chosen in an effort to determine whether or not plastic deformation might occur with higher weights. The weight was hung only a centimeter below the tip of the

beam, and the trial produced mediocre results, not tabulated as the results contained obvious experimental fallacies. The main problems arising included the beam's continuing oscillations after loading, the distance of the weight from the tip of the beam, the inability to focus the laser properly to record an accurate distance readout on the Z-axis, a time-consuming data collection method, and some minor errors involving the voltage readout on the multimeter.

When the beam was initially loaded, it continued to vibrate and oscillate for nearly fifteen minutes following weight placement. The vibrations produced hectic voltage readouts on the multimeter, as movements as small as a hundredth of a millimeter produced voltage differences of about four hundred thousandths (a large difference when dealing with such precise instrumentation). The amount of time necessary to dampen the beam's oscillations naturally, due to air resistance or its internal friction, posed a tremendous researching hurdle. The number of trials necessary made such a wait implausible if testing was to be completed within a reasonable amount of time.

Initially, the experimental procedure was to keep the traverse's Z-axis stationary and travel the length and width of the beam with the X- and Y-axes. The voltage readout would be recorded at each station, thus enabling the researcher to convert the voltage to a displacement for the Z-axis. Because the NCDT's working range spanned only five centimeters, the traverse would have to be "zeroed" whenever the NCDT had moved to a position on the beam out of its range. Zeroing the traverse means the Z-axis on the control/driver would be reset to zero after the NCDT had been moved within range of the beam again. The difference noted on the controller digital readout would indicate how far the laser had moved vertically, and the procedure would continue until the tip

displacement was recorded. However, the beam's oscillations made pinpointing precise voltage readouts a serious issue. Unless the beam was maintained in a perfectly undisturbed state, it would be extremely difficult to estimate the average digital readout produced via the multimeter, and without the measurement, all Z-axis displacements could not be recorded.

The weight, originally hung very close to the bottom of the beam's tip, caused data errors as well. The reflective steel surface interfered with that of the beam, providing inaccurate data points for Z-axis calculations. When within a range of five centimeters, the steel weight would bounce a signal back to the NCDT, producing a voltage readout equivalent to nearly two centimeters of error on the Z-axis. The error was unacceptable, as all displacements were measured to within a hundredth of a millimeter.

The targeting of each data point was an iterative process. Initially, the experimenter took data points all the way down one side of the beam from root to tip, and

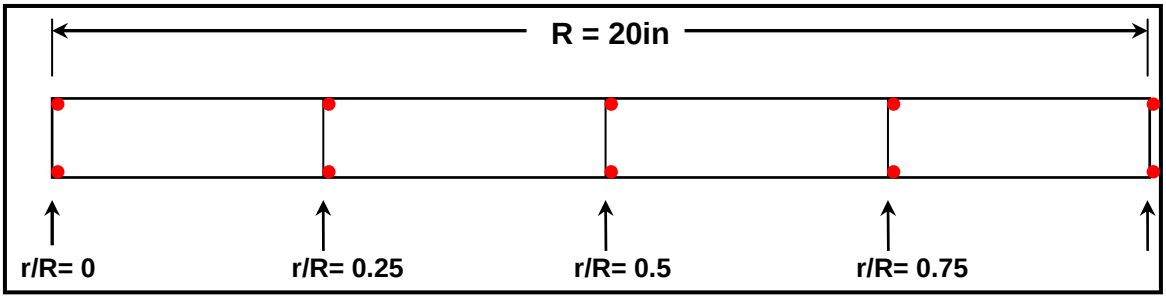

Figure 8: Data point locations

then recorded data from the other side of the beam from tip to root. The process proved to be time-consuming, but there was an obvious solution. The Y-axis displacement was the longest distance measured, so an effort was made to decrease the time traversing the major axis. Each point on one side of the beam bore nearly the same coordinates as its adjacent location. The Y and Z coordinates were nearly the same at each radial station,

thus enabling the experimenter to travel a short distance along the X-axis to gather both data points nearly simultaneously. After taking data points with one weight, the traverse was zeroed on all axes at the hub of the apparatus. The tip weight was replaced, and new displacement data were taken at the same pitch angle.

The combination of all testing errors made the initial data ultimately unusable, but the knowledge gained from initial trials helped produce a more precise method for data collection. The procedure was then refined, and all data was recorded for different beam pitch angles with numerous tip loads.

3.3.2 Procedural Improvements

Learning from past mistakes, the experimenter chose to take data collection in a slightly different direction. The weights were hung at least two inches below the tip of the beam, well out of the range of the NCDT. Once the beam was originally loaded, the vibrations were manually reduced, and the optics table and swiveling base hub apparatus were no longer contacted until the end of that trial run. The weights were replaced at the tip of the beam, before zeroing the control/driver, at the end of each trial. Starting at the hub, the data was recorded for each point at a given tip load, and at the last radial station, the weights were switched. As the beam's pitch angle remained the same between different tip loads, so did the space-fixed axes in relation to their origin. The axes' remaining fixed led to the ability to change out tip weights and record more displacement data from the final radial station to the swiveling hub. In this manner, two trials were performed every time the NCDT traveled the length of the beam and returned. The improvement reduced the time required for testing each tip load at varying pitch angles while still remaining plausible and accurate.

Because the multimeter's digital readout was somewhat erratic, it was determined that the NCDT should remain at a constant height with respect to the top of the beam. A measurement of +1.00000V became the goal for each trial. If the voltage readout was within 0.00400V, then the NCDT was focused to within 0.005mm of its proper location. In this manner, the laser distance meter never required normalizing as the beam "sunk" out of its range on the Z-axis with higher loading. Each data point was taken with a displacement error of +/- 0.005mm.

3.3.3 Revised Procedure

The procedure was revised and retried until a timely yet precise method could be implemented. Data were recorded for initial beam pitch angles (θ_o) of positive and negative fifteen, thirty, forty-five, sixty, seventy-five, and ninety degrees. Data were also recorded for zero degrees and 180º. As noted in the appendices, each of the different pitch angles carried with it a specific set of tip loads, as the original Princeton beam experiments reduced the chances of plastic deformation on the tested beam. At higher initial pitch angles, maximum tip loads were reduced from four pounds to as little as 1.5lb (Appendix A).

Positive pitch angles were tested prior to negative pitch angles for two important reasons. The traverse was positioned perpendicular to the table, and its weight and size made it extremely cumbersome to move. Thus, the NCDT could only produce displacement measurements when the beam was angled toward the meter's receiver. From the hub view, the positive angles were easily tested using the NCDT. Obviously, negative angle displacements could not be recorded as the laser's required angle to reach the receiver exceeded the angle allowed by the beam itself. In essence, the beam served

to block the NCDT's laser at negative pitch angles, and the entire apparatus, including the base column, swiveling hub, and connected beam, had to be turned 180º and reattached to the optics table so that data could be taken from the other side of the beam. Thus, both negative and positive pitch angles were tested at varying tip loads, and testing was completed using a revised method for traveling the length of the beam.

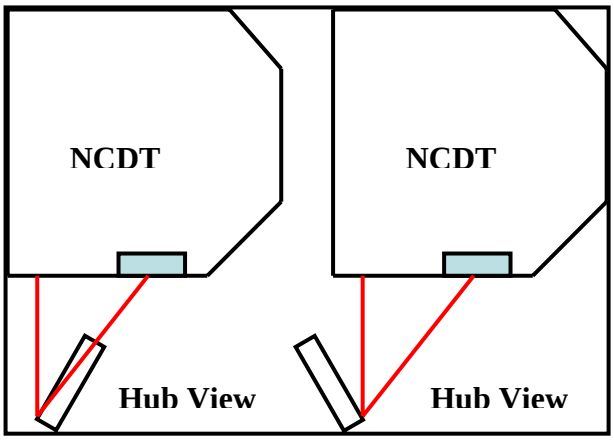

Figure 9: NCDT angular disadvantage

To "fix" the correct angles during testing, the beam was bolted to the swiveling hub, and the inclinometer was activated. The digital readout produced angular measurements accurate to +/- 0.005˚, and once the apparatus was swiveled to the required angle, the hub was tightened to the column and left stationary until all tip loads were tested. The inclinometer's range of fifty degrees made it impossible to measure increasing inclines, so the inclinometer was unbolted from the swiveling hub and reattached at a position plus or minus ninety degrees of its original location. Simple subtraction determined the hub's base angle, and all angles could be accounted for.

For positive pitch angles, the NCDT was focused on the left side of the beam, with reference to the hub view. This was considered its "zero point," or origin, for all data at that initial pitch angle. The control/driver was normalized to this point, as all

axes were zeroed. From the origin, the traverse was manually controlled along the X axis to record the opposing data point at the hub. Throughout each trial at a given pitch angle, these two points remained the same for varying tip loads, and were not retested for every tip load. The traverse was then maneuvered down the length of the beam toward the first radial station, at which point the displacements were recorded for both edges of the beam widthwise. When all of the radial stations had been tested, the traverse remained at the tip of the aluminum beam, at which time the tip load was increased, and the beam's oscillations were manually damped again. Data were recorded returning to the first radial station, as the root coordinates remained the same, and all data were compiled for the required tip loads. The traverse was eventually returned to the origin at the hub to ensure the trial was performed while maintaining the correct special axes. If the traverse motors slipped or the controller miscalculated the displacements, the origin had moved, and the trial was completed a second time. The check helped to ensure that all data remained accurate. Negative pitch angles were tested in the same manner as positive angles, with a backwards system of axes.

The control/driver produced digital readouts as high as ten thousand millimeters, much higher than the traverse's capable distance. So, for all positive readouts on the controller, numbers were produced normally. However, for negative readouts, coordinates were produced in terms of ten thousand millimeters minus the distance traveled. The coordinates were then produced in terms of negative and positive distance from the origin.

Following all data collection, the coordinates were reproduced in terms of the beam's elastic axis, forming a set of five data points for each tip load at a given angle.

The X and Z coordinates were used with the tangent function to calculate the beam's angular displacements at each radial station, and the plots produced showed trends and were compared with Princeton beam data.

4. Results and Analysis

4.1 Deflection Analyses

The data recorded for each trial is tabulated in Appendix B, and the data reproduced in terms of the beam's elastic axis has been tabulated in Appendix A. All angles with corresponding tip loads were tested (Appendix A), and figures were produced using the data calculated. However, in the interest of discussing correlations between X-axis, Y-axis, Z-axis, and angular deflections, figures were produced for positive and negative thirty, sixty, and ninety degrees for each of these cases. The trends can be assumed to be indicative of trends at all pitch angles and tip loads, but all angular tests are not represented visually in this section.

4.1.1 X Axis Deflection

The X-axis deflections for positive and negative zero, thirty, sixty, and ninety degrees are represented here for all respective tip loads between zero and four pounds. All data show an initial offset from the origin, possibly due to machining deformations prior to testing.

Deflections at a pitch angle of zero degrees (Figure 10) were performed for tip loads between zero and four pounds in one pound increments. The beam moves thirty millimeters in the negative X direction at four pounds, because it tends to remain vertical, with respect to the tip view, during deformations. However, because the beam has initial machining stresses, it does move slightly along the X-axis, where as the Princeton beam experiments assumed a stationary X-axis deformation for the beam at zero degrees. The

tip deflection at zero pounds also begins about fifteen millimeters from the origin, another indication of initial beam deformations.

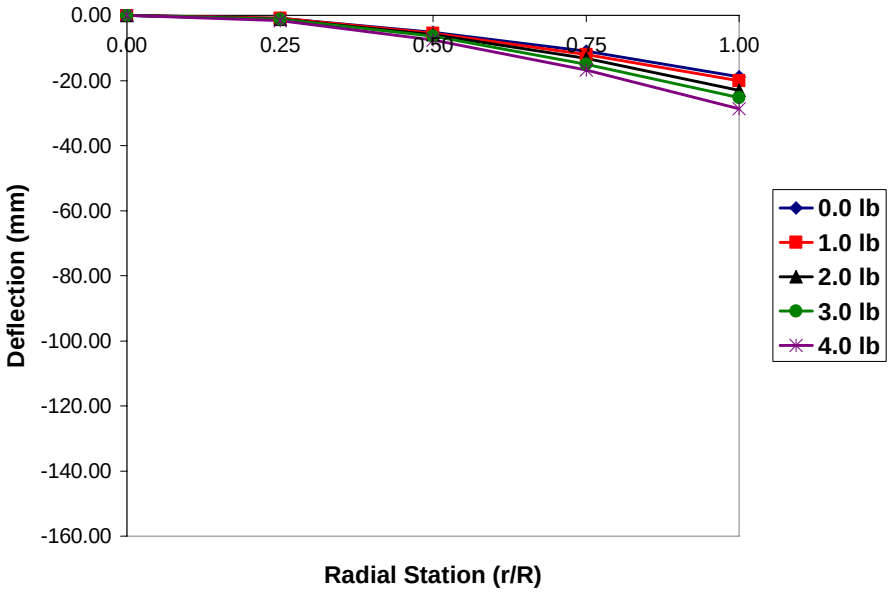

Figure 10: X Deflection (0 deg)

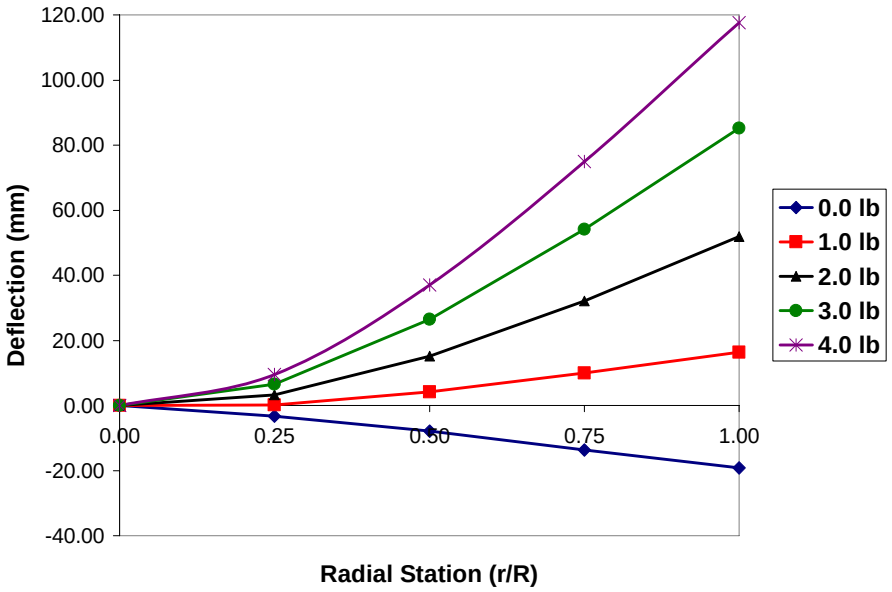

Figure 11: X Deflection (30 deg)

The positive and negative thirty degree pitch angle trials (Figures 11 and 12) were performed between zero and four pounds in one pound increments. For an initial pitch

angle of thirty degrees, the maximum X deflection reaches nearly 120mm, or about 105mm farther than the maximum deflection at zero degrees. The zero pound tip load actually shows a negative X deflection, but the maximum deformed state is assumed at the four pound tip load as it is for the negative thirty degree pitch angle.

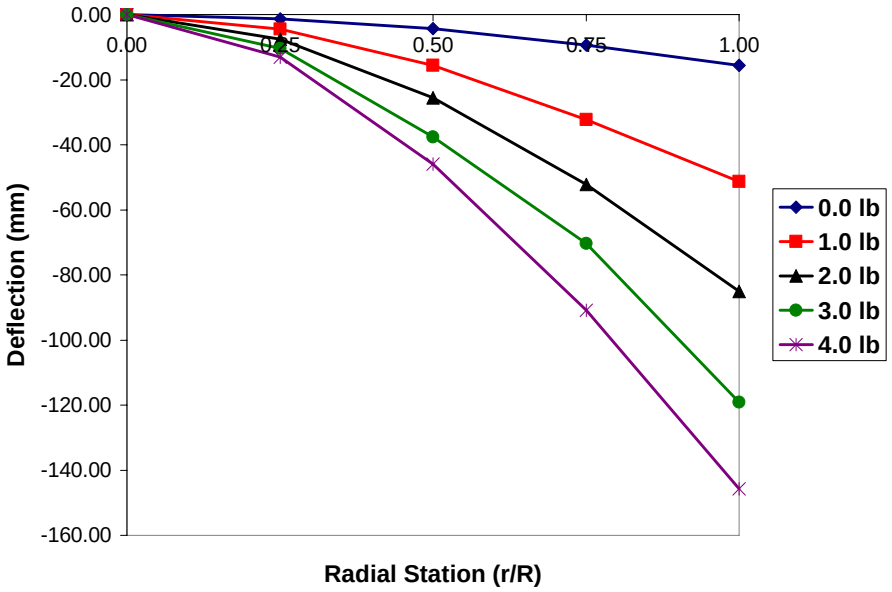

Figure 12: X Deflection (-30 deg)

Both pitch angles, however, show a maximum deformation of about 135mm from the beam's unloaded state, indicating that the beam's displacements are similar regardless of its pitch angle's positivity or negativity. Such a correlation suggests that the beam's maximum deflections differ due to initial deformations.

At positive and negative sixty degrees (Figures 13 and 14), the beam was loaded between zero and two pounds in half pound increments. The beam tends to deflect a shorter distance along the X-axis than it does at thirty degrees. The main reason for such a difference is due to the transference of the beam's loading from an angle closer to the vertical to an angle closer to the horizontal axis. At zero degrees, the beam deflects very

little in the Z direction, whereas the beam deforms greatly in the Z direction. The beam transfers its vertical load from the X-axis to the Z-axis as pitch angles increase. The sixty degree trials show a more exaggerated deflection in the Z direction while the thirty degree trial will not produce large Z-axis deflections. Thus, the beam deflects

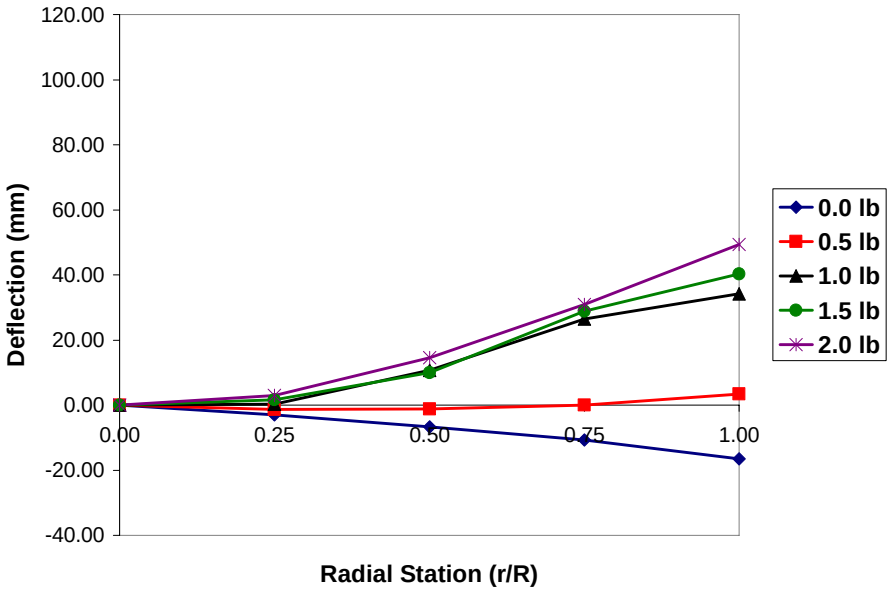

Figure 13: X Deflection (60 deg)

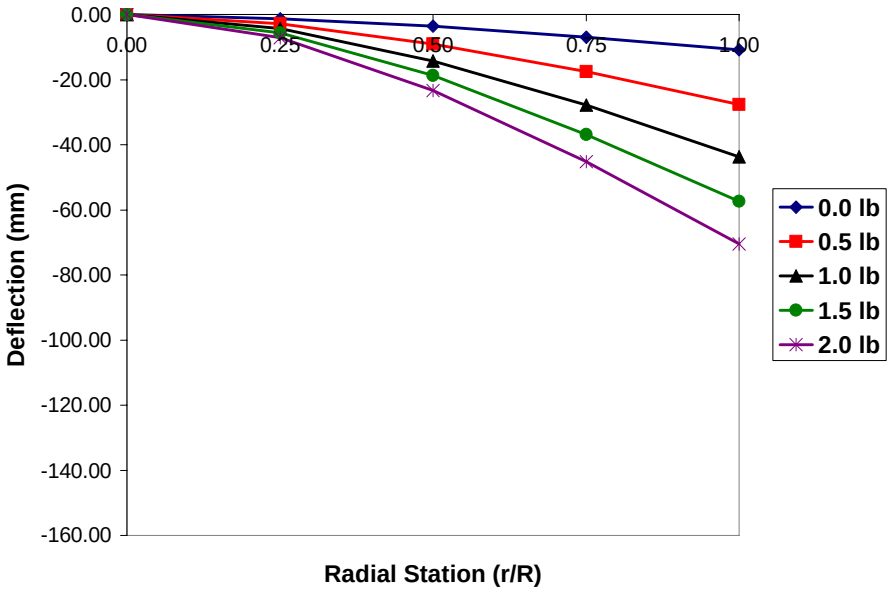

Figure 14: X Deflection (-60 deg)

approximately sixty millimeters from the unloaded origin for both pitch angles. Both of the trials also have an initial offset from the origin, again due to beam deformations.

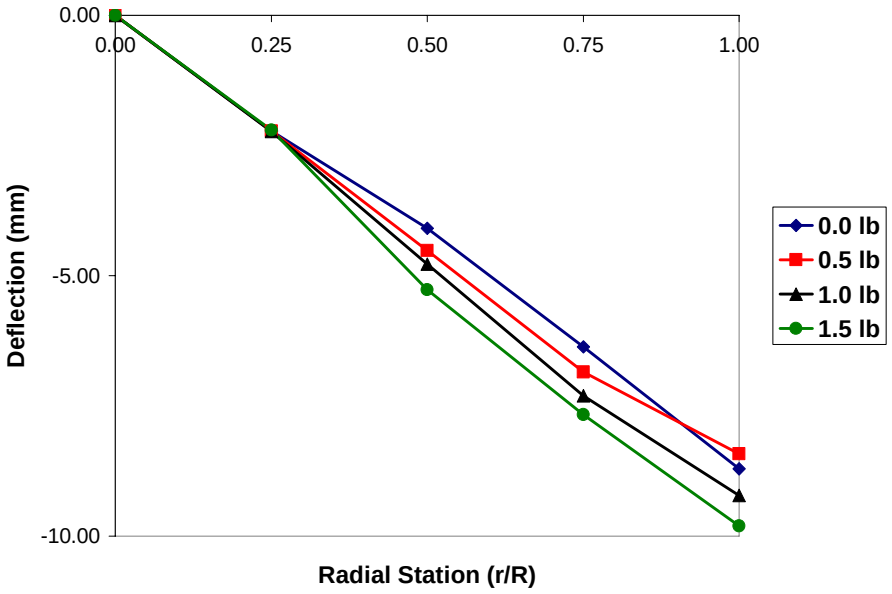

Figure 15: X Deflection (90 deg)

Tip loads between zero and 1.5lb in half pound increments were loaded on to the positive ninety degree pitch angle trial (Figure 15). Here, less weight allowed the beam to deform without the risk of plastic deformation. The beam shows negligible X-axis deformations of no more than ten millimeters. Again, the largest deflections occur for the largest tip loads, and the trends remain constant for all data presented. Figure 15's axes have been enlarged to show the deflections at each radial station, so they are not presented on the same scale as the previous figures representing X-axis deflections.

4.1.2 Z Axis Deflection

The Z-, or vertical, axis deflections were greatest for the higher positive and negative pitch angles, just as the lower pitch angles produced the highest X deflections.

As the pitch angle increases, the tip load's effect tends to progress from the X-axis to the Z-axis (evident for pitch angles of zero degrees as well).

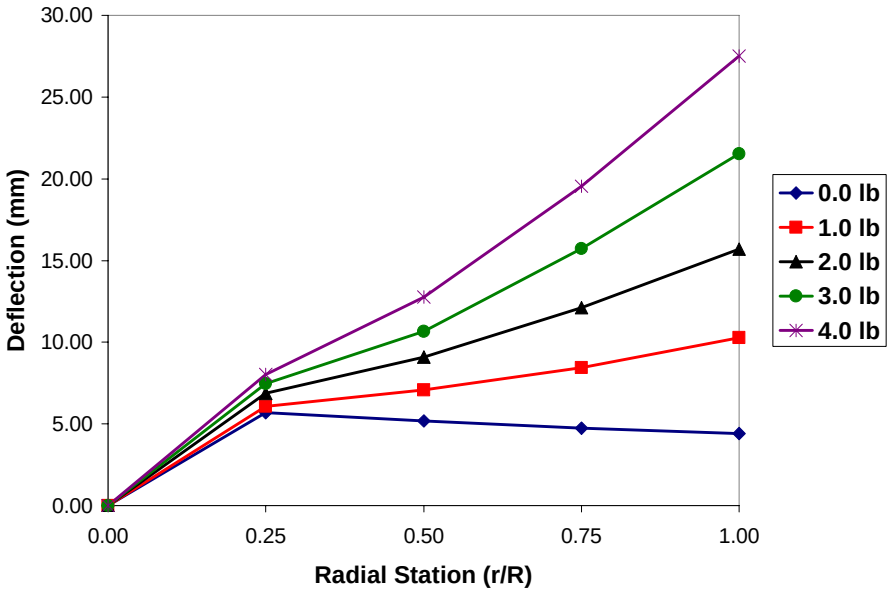

Figure 16: Z Deflection (0 deg)

At zero degrees (Figure 16), a Z deflection of approximately twenty-seven millimeters occurs at the final radial station for the maximum tip load. The beam's deformation data differs somewhat from those in the Princeton beam experiments which assumed the beam had zero deflection, along the X- and Z-axes, in its unloaded state.

The thirty degree trials (Figures 17 and 18) show a Z deflection of a little more than one hundred millimeters from the beam's unloaded state to its fully loaded state of four pounds for positive and negative pitch angles. The greatest deflections occur at the greatest tip loads, and deflections between zero and four pound loads increase with loads as well. The negative pitch angle data's correlations resemble the positive pitch angle data almost precisely, implying that the beam again deflects in nearly the same manner for positive and negative angles regardless of machining stresses. The negative pitch

angle obviously promotes a larger Z-axis deflection, as this is the direction of the beam's original warping along its length.

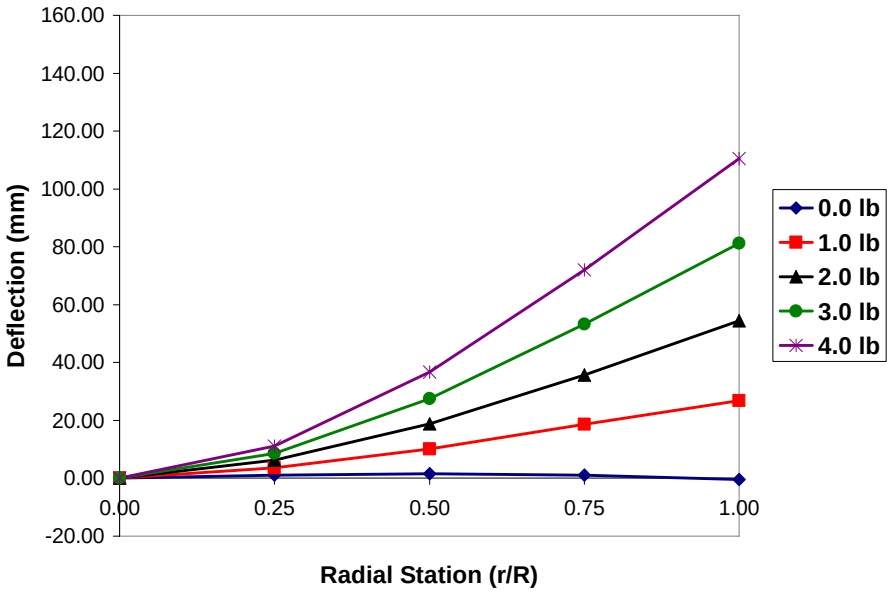

Figure 17: Z Deflection (30 deg)

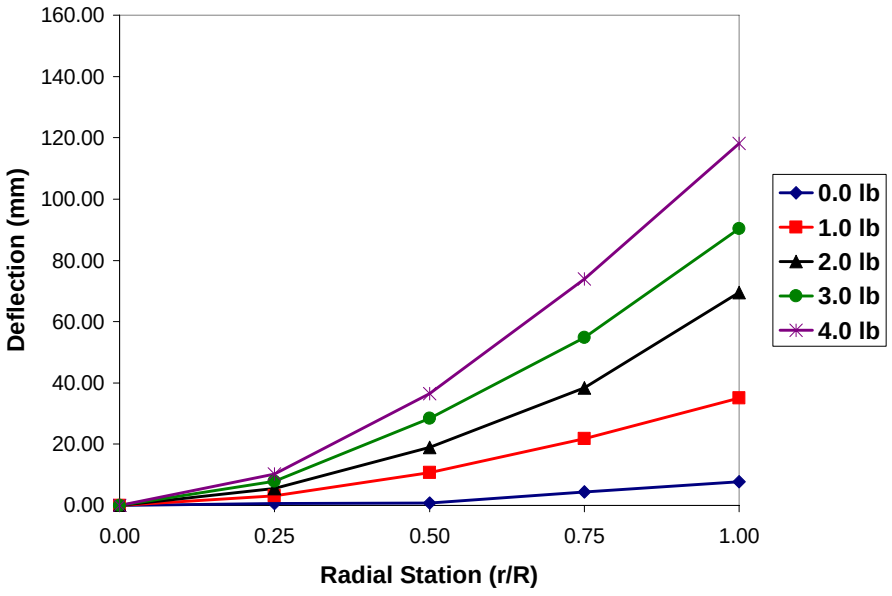

Figure 18: Z Deflection (-30 deg)

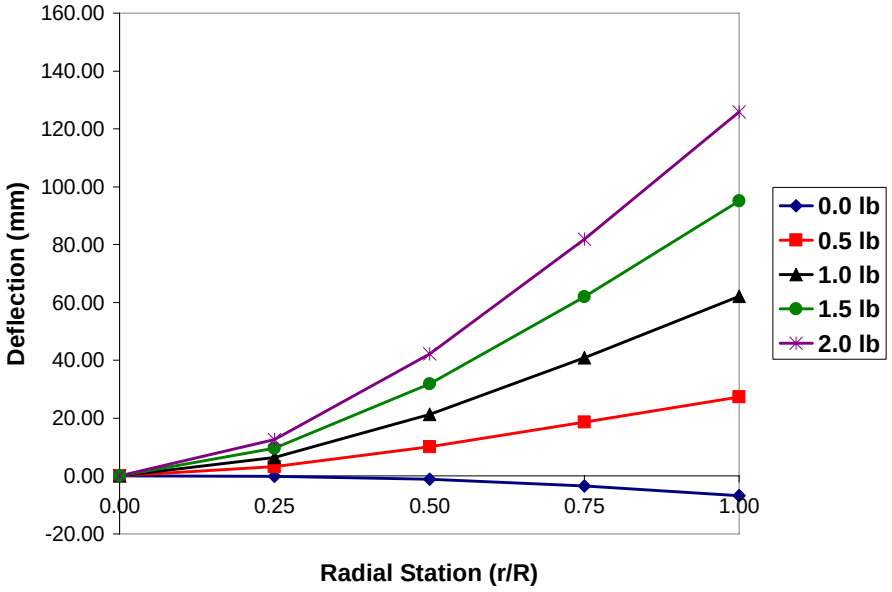

Figure 19: Z Deflection (60 deg)

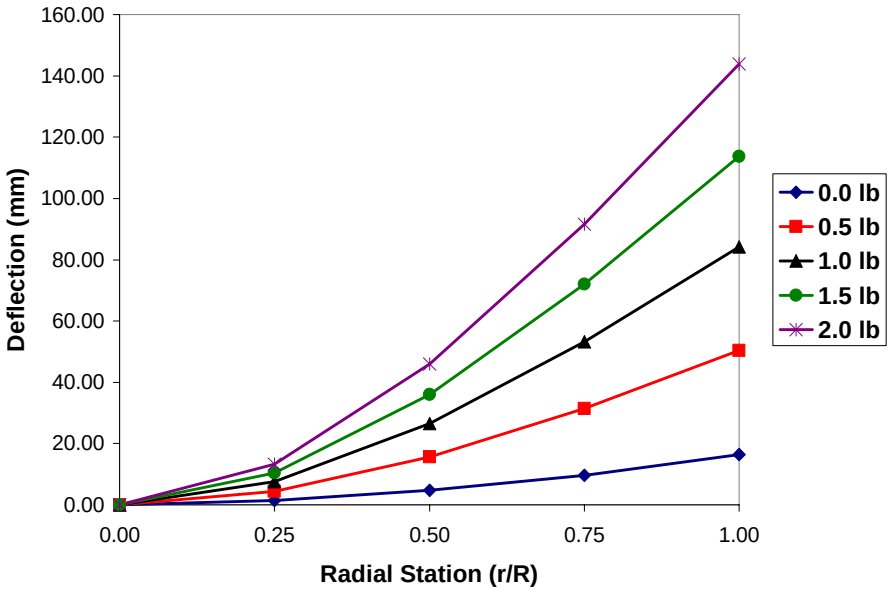

Figure 20: Z Deflection (-60 deg)

As predicted, the positive and negative sixty degree pitch angles (Figures 19 and 20) result in larger Z deflections than do the thirty degree trials. At its greatest tip load and radial station, the positive test produces a deflection of almost 140mm from its

original unload state. The negative trial shows a maximum deflection of approximately 140mm as well, and Figures 19 and 20 add more credit to the assumption that increasing pitch angles show decreasing X deflections and increasing Z deflections. Figures 19 and 20 indicate the same basic results as all other figures produced, with increasing tip loads promoting increasing Z-axis deflections. It stands to reason that the positive trial will show and initial negative (upward) deflection along the Z-axis, because the beam's original warping causes it to do so. However, the negative trial shows an initial positive deflection.

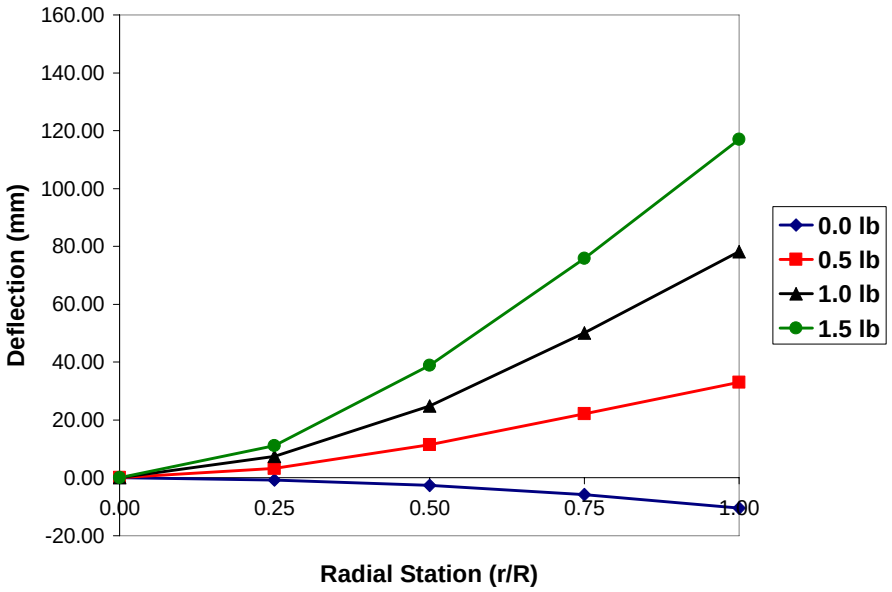

Figure 21: Z Deflection (90 deg)

The ninety degree trial (Figure 21) shows large elastic deformations for increasing tip loads. Figure 21's deflections reach about 130mm in displacement at the maximum, and again the two different pitch angles produced very similar deflection data.

4.1.3 Angular Deflection

As previously discussed, the positive and negative pitch angle trials tend to present the same results, and will henceforth be produced in terms of only the positive pitch angle trials of thirty, sixty, and ninety degrees. The zero degree trial was assumed to have pitch angle displacements of zero degrees. Obviously, if the beam produced X axis displacements at zero degrees, there was some amount of pitch angle deformation. However, given the setup, the NCDT could not be properly positioned to find such small angles. The scatter among the data points is due to experimental error, and will be addressed.

At thirty degrees (Figure 22), the greatest angular deflection, unsurprisingly, occurs at the greatest tip load of four pounds. The pitch angle changes over a range of about seven degrees from the beam's unloaded position to its loaded position.

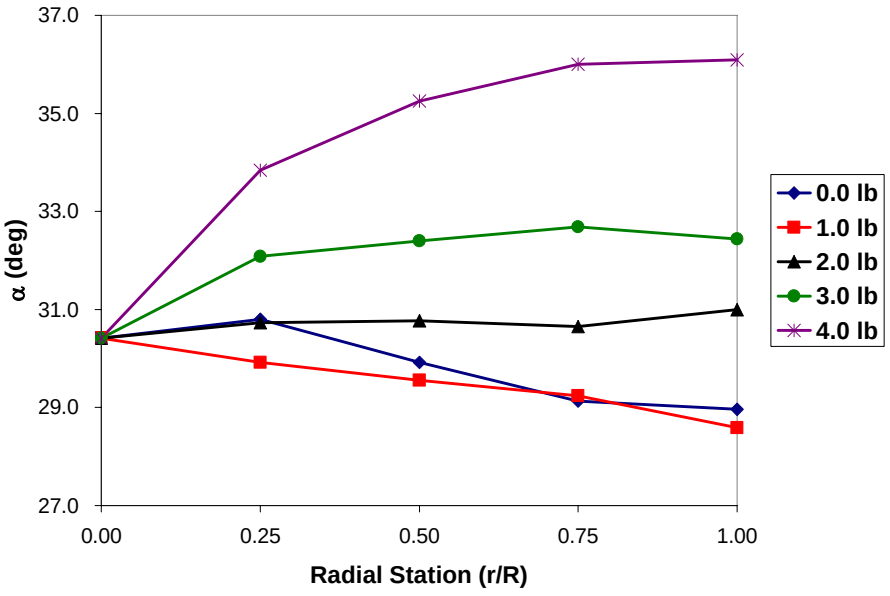

Figure 22: Angular Deflection (30 deg)

At sixty degrees (Figure 23), the pitch angle changes very little. The scatter makes deducing trends from Figure 23 relatively difficult, but the relative angular tip

deformations remain between about zero and two degrees consistently. At lower pitch angles, the angular deflection tends to be greater among all the trials, thus implying that a larger X deflection will serve to produce a larger angular deflection as well.

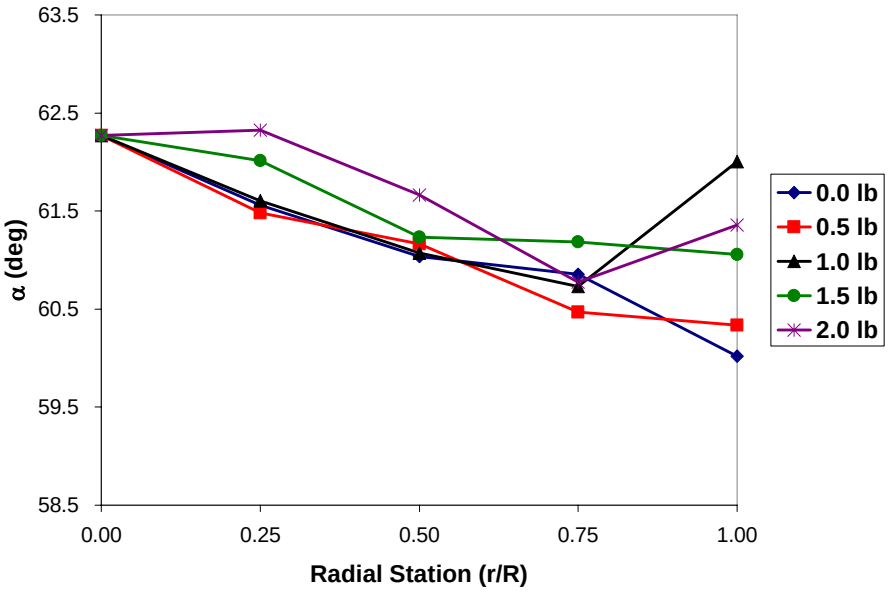

Figure 23: Angular Deflection (60 deg)

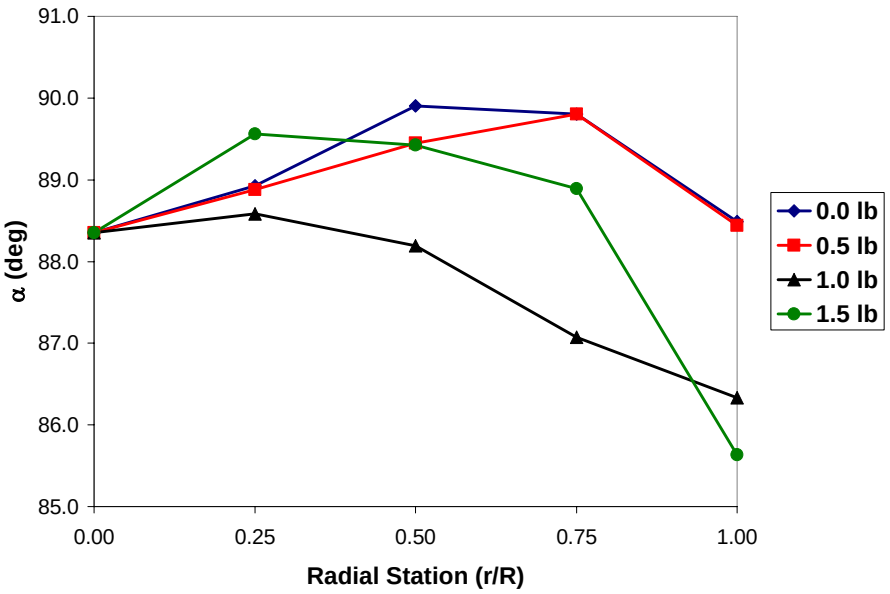

Figure 24: Angular Deflection (90 deg)

At ninety degrees (Figure 24), any angular deformations will occur only because of machining stresses. The Princeton Beam Experiments automatically assumed no angular deflections for a pitch angle of ninety degrees, but these deflections seem to follow a relatively obvious trend. At higher tip loads, a beam pitch angle of ninety degrees produces the highest angular deformations at a tip load of 1.5lb, as it should.

4.1.4 Tip Load Comparisons

The tip load comparisons are a combination of the zero, thirty, sixty, and ninety degree trials. All deflection data are in terms of the final radial station and are presented to compare X, Z, and angular deflections for all trials from zero to ninety degrees.

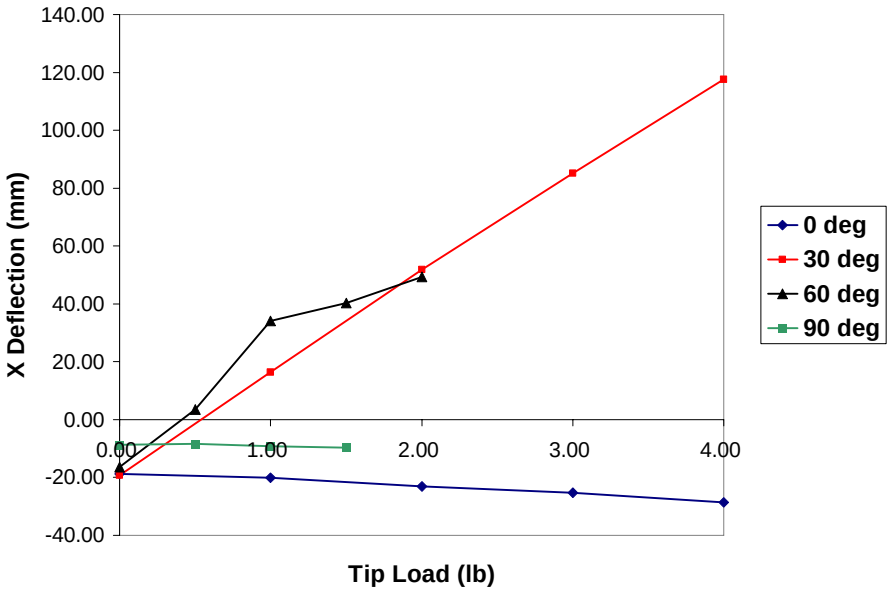

Figure 25: Tip Load v Tip X Deflection

As expected, the zero and ninety degree trials have very little maximum X deflections in comparison with the other beam pitch angles (Figure 25). At thirty degrees, the X displacement increases at a rate slightly greater than that of the X

displacement at sixty degrees. This stands to reason, as the experimenter has found that the lower the pitch angle, the higher the X deflection.

The tip Y-axis deflection at different pitch angles (Figure 26) can be related to the maximum Z displacement the beam reaches at its highest loads. The higher the pitch angle, the greater the Z deflection, and so the Y, or lengthwise, deflection tends to increase as well. At zero degrees, the Y deflection remains close to the origin, and at ninety degrees the Y displacement increases more rapidly with maximum tip loading.

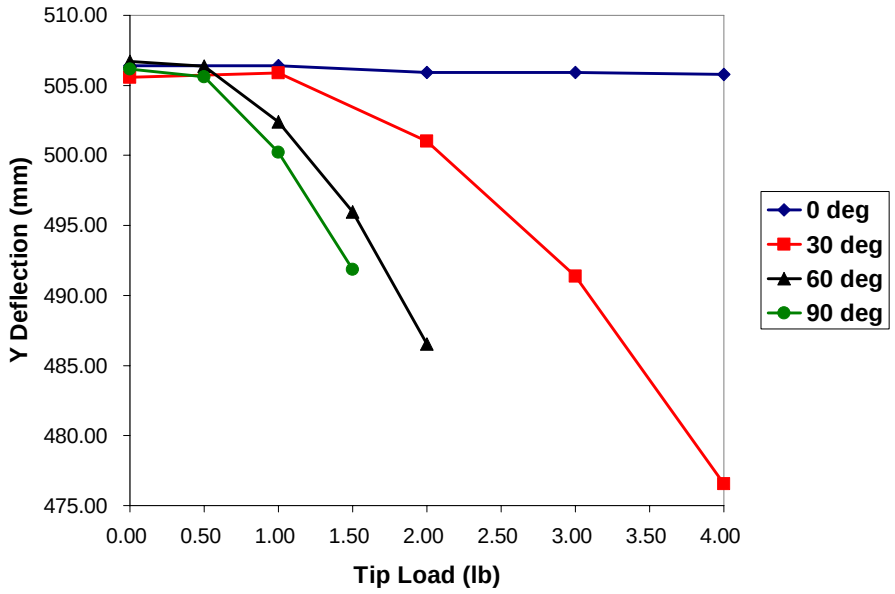

Figure 26: Tip Load v Tip Y Deflection

The Z-axis tip load displacements (Figure 27) appear as expected, considering increasing pitch angles "flatten" the beam, making it more susceptible to vertical deflections as opposed to horizontal deflections, assuming a tip view of the beam. The more "upright" or vertical the beam is placed, the more likely it is to deform along the X-axis. However, the beam's increasing pitch angles increase its Z displacement measurements as its inertia travels from the X-axis to the Z-axis.

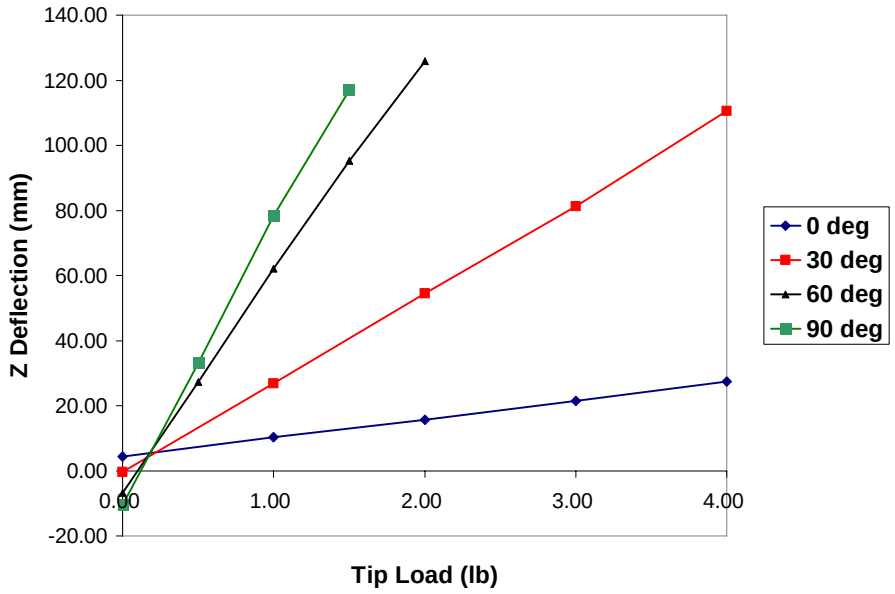

Figure 27: Tip Load v Tip Z Deflection

Upon examining a visualization of tip angle deflections with respect to tip loads on the beam (Figure 28), it becomes apparent that angular displacements vary only slightly between differing pitch angles. There appear to be little to no correlations between changing initial pitch angles and there subsequent deviations.

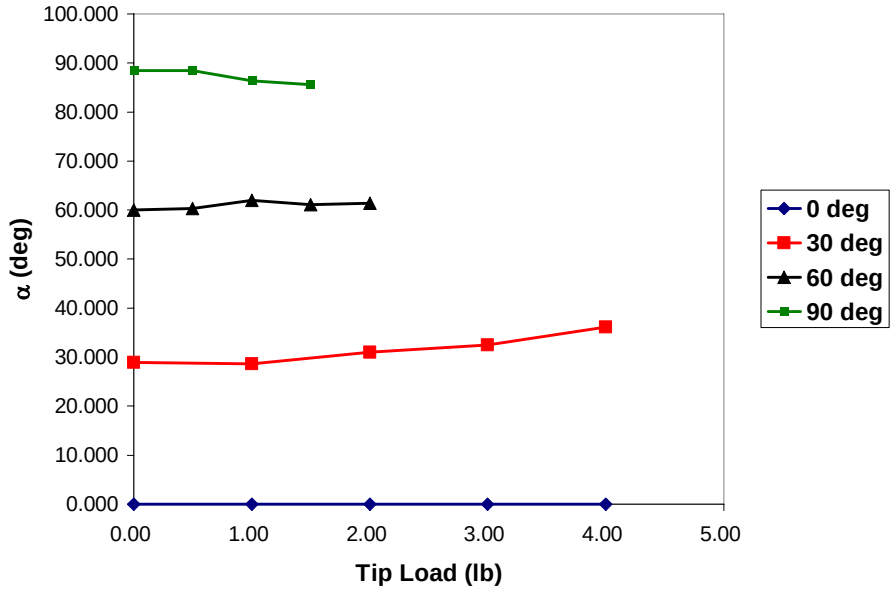

Figure 28: Tip Load v Tip Pitch Angle Deflection

4.2 Comparison with Princeton Beam Data

Tabulated in English units in Appendix C, the Princeton beam data has been sampled to produce comparisons between current tip data (from this experiment) and the Princeton beam experiments of 1975. To allow the comparison, the data requires compatibility, so all recorded Princeton beam data has been converted to millimeters, and all current data is recalculated in terms of the Princeton beam experiment's original assumptions. In essence, the current tip deflection data for a load of zero pounds does not reflect a beam without initial deformations as the Princeton beam experiments do. Therefore, all unloaded tip deflections differ from the origin on the X- and Z-axes, and the differences for these data points has been taken in to account for comparisons to Princeton beam data. The same is true for all angular comparisons, as initial beam angles did not necessarily equal the assumed pitch angles of those in 1975. The calculated initial pitch angles for current data are recorded in Appendix A.

The similarities between Princeton beam experiment results and current results are undeniable. Because there were no Y deflection results in 1975, those correlations cannot be reproduced here. However, the X, Z, and angular deflections obviously bear an uncanny resemblance to the data previously produced, seemingly validating both the current experiment and past experiments as well. The X deflection data for initial pitch angles of positive and negative thirty degrees (Figure 29) deviate from Princeton beam data as the current X-axis deflections are larger than deflections from 1975. A positive pitch angle of thirty degrees produces a difference, between current data and Princeton beam data, of nearly twenty millimeters. Figure 30 shows a comparison between

Princeton beam experimental and current tip deflections as well. Again, the current displacements are larger than Princeton beam experimental X-axis deflections.

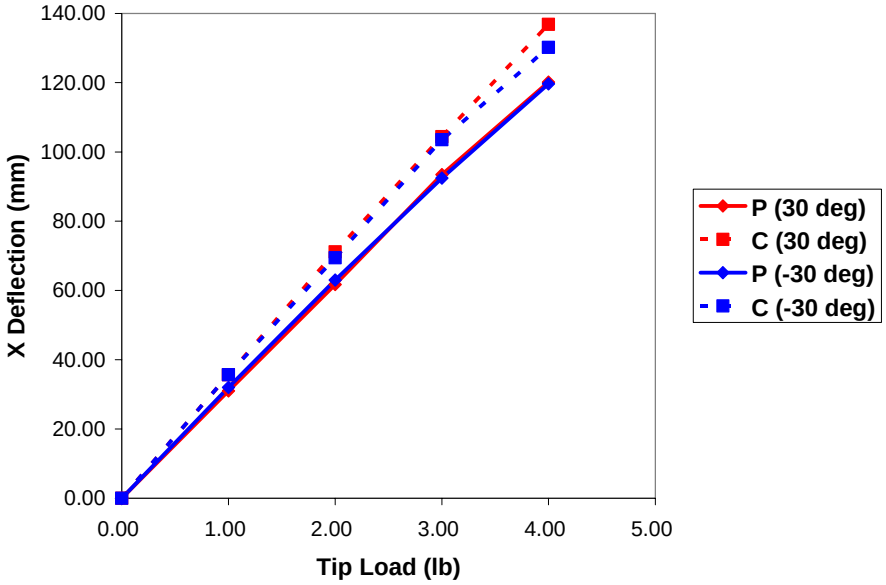

Figure 29: X Comparison of +/- 30 deg trials

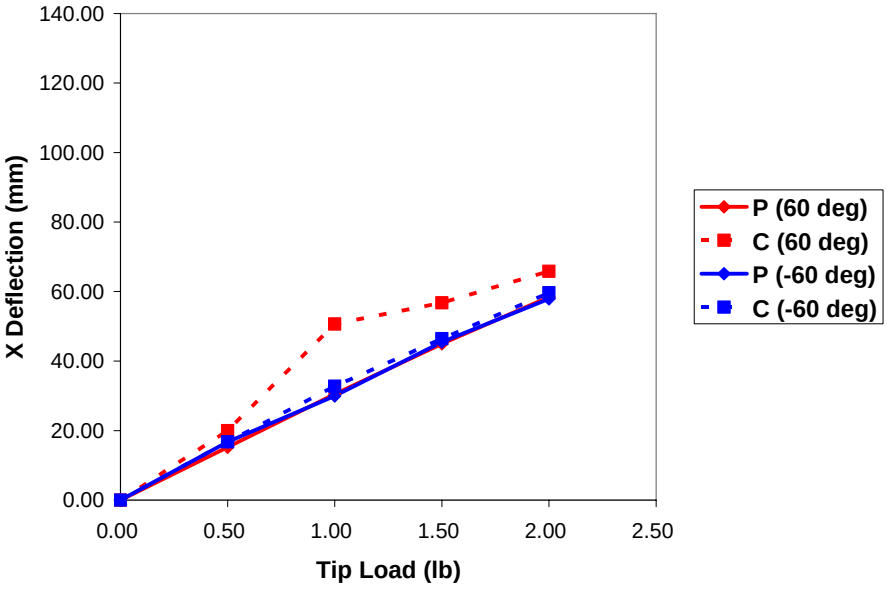

Figure 30: X Comparison of +/- 60 deg trials

The same displacement increase from 1975's data to present data is evident for Z displacement measurements as well (Figures 31 and 32). Data from the final radial

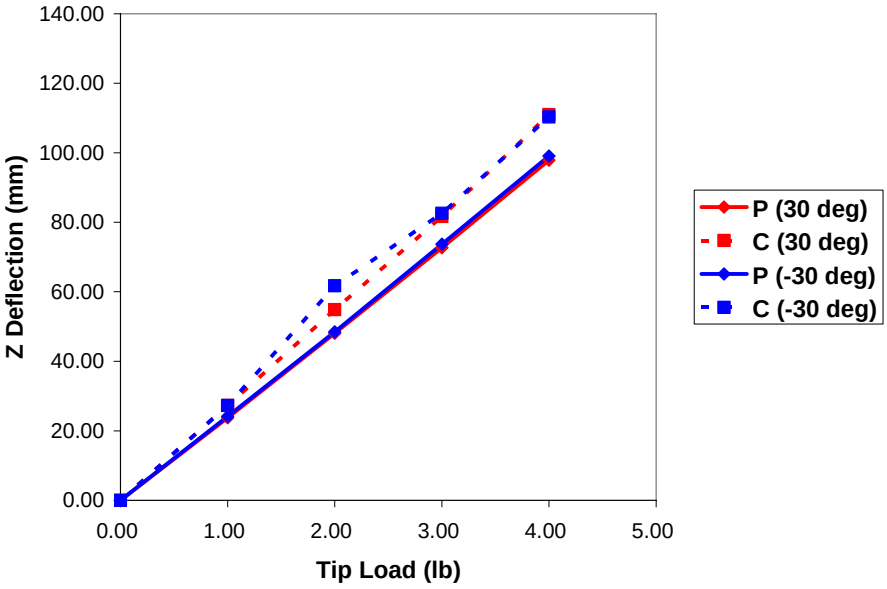

Figure 31: Z Comparison of +/-30 deg trials

station at different pitch angles can be considered the most extreme deformations the beam will undergo, so the comparison between the Princeton beam data and current data were performed at the last radial station of the deflected beam. The current Z-axis displacements for positive and negative thirty degrees (Figure 31) have increased over displacements measured in 1975 by approximately ten millimeters. For pitch angles of positive and negative sixty degrees (Figure 32), the increase in displacement measures about twenty millimeters for the maximum. The overall increase in current beam displacements is evident for pitch angles of both positive and negative thirty and sixty degrees.

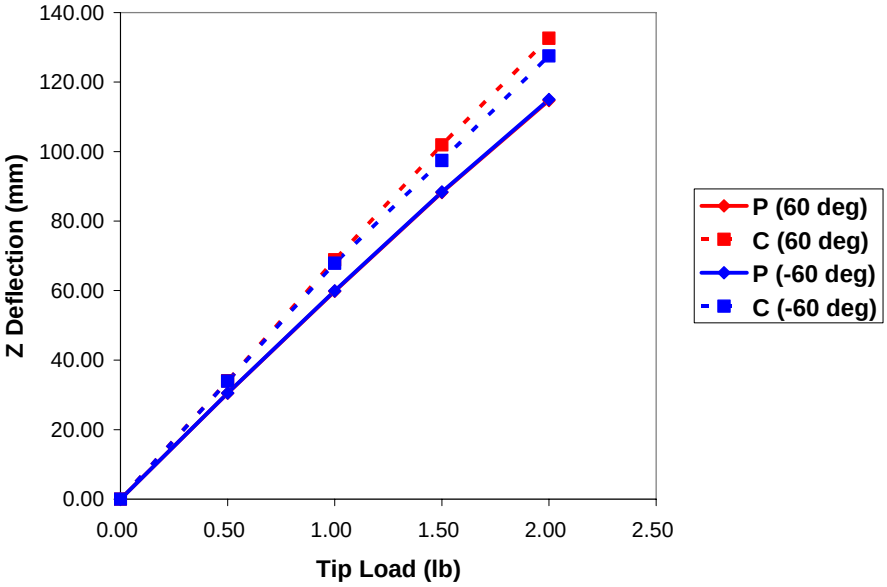

Figure 32: Z Comparison of +/-60 deg trials

Tip angular displacements for current data and Princeton beam data have been compared for thirty and sixty degree trials as well (Figures 33 and 34). The negative pitch angles are reproduced as positive angular displacements for comparison purposes.

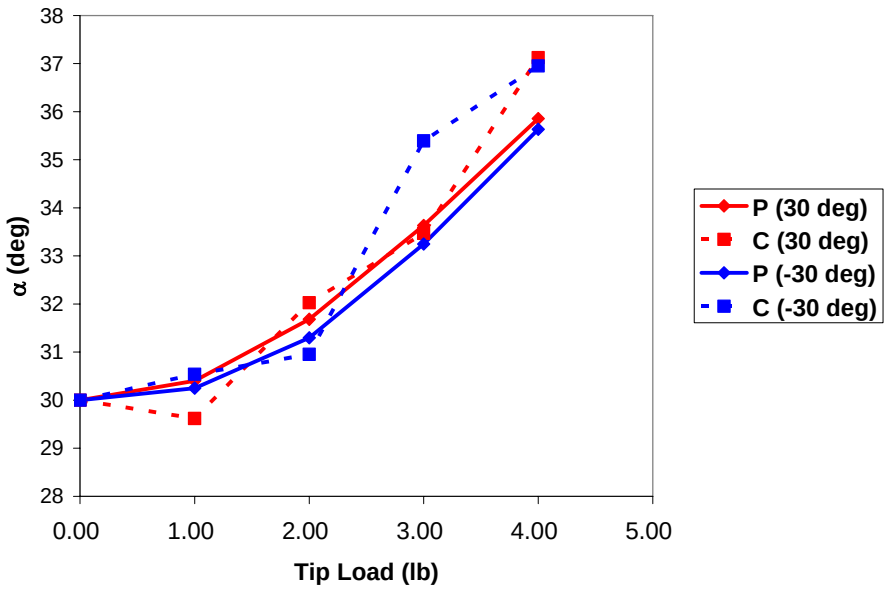

Figure 33: Angular Comparison of +/- 30 deg trials

As expected, the positive and negative angular displacements for both trials have increased over those from 1975. The thirty degree trials (Figure 33) show a larger angular displacement (approximately seven degrees) than do the sixty degree trials (Figure 34) with a displacement of just two degrees. As an extreme example, the higher initial pitch angle trials, such as ninety degrees, will produce little to no tip angular displacements with increasing loads. At ninety degrees, the beam is deflecting almost entirely in the Z direction as its inertia is not opposed on the X-axis.

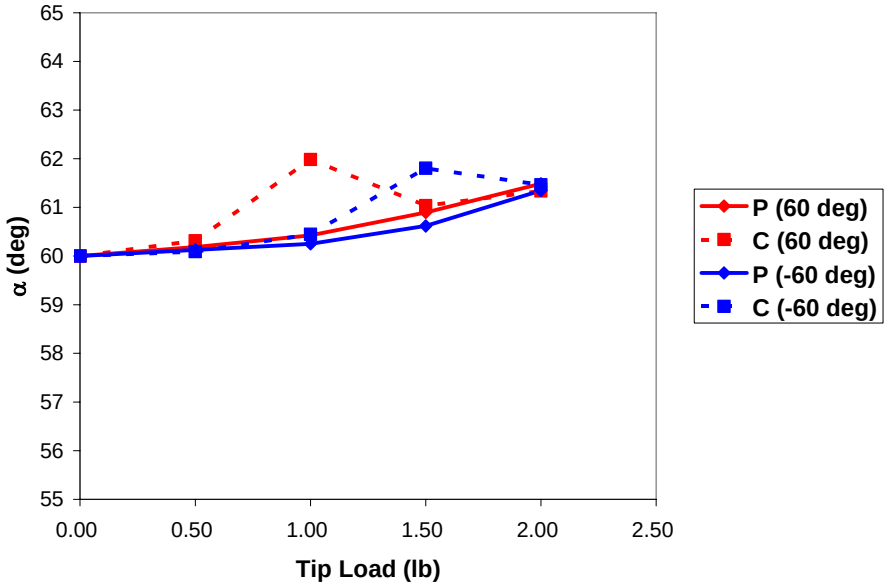

Figure 34: Angular Comparison of +/- 60 deg trials

4.3 General Analyses

The most notable differences between Princeton beam displacement data and current displacement data, aside from the current beam's initial curvature, deal with an overall increase in X, Z, and angular displacements. Both beams are machined to the same dimensions using a sheet of 7075 aluminum. The temperatures of past and present testing facilities are assumed to remain constant, and both methods of testing seem to be

accurate with only differences in precision. The current beam's tendency to deflect between ten and twenty millimeters farther than past data must be due to a change in material properties, experimental procedures, or beam geometries. The current beam was produced with the same dimensions as the beam from 1975, and the present beam's curvature was taken in to account for the Princeton beam data comparisons (Figures 29-34). So, the machining processes and the beam's geometry probably have very little to do with the differences between the two sets of displacement data. The two methods for beam testing have produced precise nonlinear deformation data, and there is no reason to assume that either method's data are inaccurate. So, the present displacement increases most likely result from experimental differences and material property discrepancies. Error bars are not included in the figures, as the precisions are too small to be visible for both Princeton beam data and current data. The displacement sets lie too far away from one another to be accounted for with error bars.

Dowell and Traybar performed the Princeton beam experiments by sliding a cylindrical weight onto the tip of the beam for both static and vibration testing. The current experiment incorporates a small screw on the tip of the beam from which the weights are hung to produce a point load. Assuming the weights for each experiment are of the same mass, one may assume that a weight slid over the tip of the beam will produce less torque than a weight hung directly from the tip. The closer to the hub a weight is applied to the beam, the less the beam will deflect. In the current case, a larger displacement occurs when the weight deflects the beam, so the weight placement accounts partly for the increased displacements for current data.

Material properties may also account for the displacement differences as well. The 7075 aluminum beam from 1975 may have been constructed via different methods than the current aluminum beam, including drawing, extruding, rolling, smelting, and refining. There is no way to determine how the beam was produced in 1975, and the current beam is cut from a sheet of aluminum, so it is most likely rolled. The moduli of elasticity, moments of inertia, and beam densities will change with different machining processes.

4.4 Linear v Nonlinear

To ensure the current beam displacements represent nonlinear deflections, a simple comparison between linear and nonlinear tip deflections is warranted. Figure 35 shows a tip deflection comparison for an initial pitch angle of ninety degrees. It is

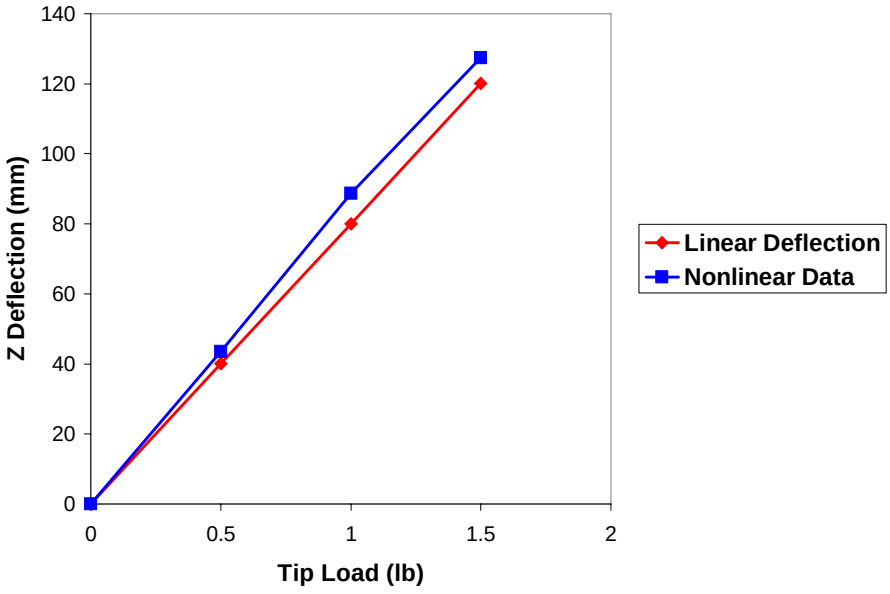

Figure 35: Linear v nonlinear (90 deg)

evident that the experimental data exceeds the linear deflection region by approximately ten millimeters at 1.5lb, and because the trial has deflected the beam to the nonlinear

region, it makes sense that increasing loads for other trials (smaller pitch angles) will produce nonlinear deflections as well. The loads for the ninety degree trial remain smaller than two pounds to ensure the beam will not plastically deform during testing.

4.5 Measurement Errors

By inspection, there are data points in the provided plots that do not follow the trends as smoothly as Princeton beam deflection data. Figures 30-34 show displacement data for the X, Z, and angular displacement trials for both current tip deflections and Princeton tip deflections. In Figure 30, there is a measurement error for a tip load of one pound on the current positive sixty degree trial. The misplaced point on the plot stands out, as do the strange scatters in Figures 31, 33, and 34. Princeton beam data is nearly the same for each of its positive and negative pitch angle trials, some times so close that one data set cannot be distinguished from the other. The cause of the scattered data for current data is therefore due to measurement error.

The traverse, as mentioned, has a tendency to stall while is moves from one point to another along the X-axis. The problem is that while the screws for the traveling X-axis have locked, stopping the traverse's motion, the control/driver continues to account for a displacement along the X-axis. The motors for the traverse are linked directly to the control/driver, and the motors will provide screw revolution data, in terms of thread displacement in the X direction, with or without the traverse's actually having moved. The traverse is relatively old, so there may be frictional losses along any of its axes, and such losses will produce less than valuable data for an experiment in which precision improvements are the main goal.

Other sources of error include the actual precisions to which the control/driver and NCDT are designed. The X- and Z-axis displacement measurement precisions are noted in Table 1. Given the precisions from the Princeton beam experiments, it is evident that the current X and Z displacement measurements have improved in precision over past data. Y displacement precisions are not noted here, because the Y-axis measurements cannot be compared with past data. However, lengthwise displacements are assumed to incorporate the same precisions as X- and Z-axis data.

Table 1: Current v Princeton precision

Deflection Axis	Precision (+/- mm)	
	Princeton	Current
X	0.254	0.005
Z	0.0254	0.005

5. Summary

To produce a more precise data set than that recorded in 1975, newer technologies, procedures, and assumptions were incorporated in to the already-existing Princeton beam experiment methods. The precisions (Table 1) were greatly increased, but the procedures themselves may have produced less than accurate data. The results showed inaccurate scatters in many of the X deflection plots, which in turn affected the accuracy of pitch angle displacement data, calculated from both Z and X coordinates. The current procedure was sound but could be improved for more accurate displacement measurements while maintaining the same level of precision. Accurate and precise results will allow more definite computer model comparisons for nonlinear beam deformations.

5.1 Future Improvements

The current procedure was sound for precise data, but accuracy improvements were needed. The swiveling hub could be redesigned as a mechanical hub, incorporating a high gear ratio and a crank to swivel the hub slowly to reach the desired initial pitch angle. The inclinometer could be attached to the hub differently as well. The current method used a small aluminum plate to bolt the inclinometer at perpendicular angles to the hub. It may be noted, from Figure 27, that the actual pitch angles for the current experiment were not as accurate as possible. By reattaching the inclinometer and adding a mechanical aspect to the swiveling hub, static and vibration testing would show overall improvements in terms of accuracy.

The tested beam's machining methods should also be taken in to account, as rolling or heating aluminum will change its material properties and resistance to

deflection. The beam's dimensions should also be studied, as different machining tolerances may affect its mass and moment of inertia.

To improve testing procedures, the experiment should be performed in a few different ways. Instead of testing the beam at one pitch angle and varying loads, perhaps the experiment should also be performed with a single load at different pitch angles so that the two data sets can be compared for accuracy. A single pitch angle should be tested more than once so that an average displacement can be calculated at each radial station, creating a set of data less sensitive to measurement errors present in individual trials. The current procedure was only performed once at each pitch angle, and the plots show measurement errors.

The NCDT received data within a range of only five centimeters, but current NCDTs are capable of operating within a twenty centimeter range. Using an NCDT with a wider range would eliminate the need to position the laser at the same height above the beam for every data point. Traverse malfunctions on the Z-axis would no longer be an issue. Voltage outputs from the multimeter would then be recalculated as displacement measurements, increasing precision.

A newer traverse could be used for static deflection testing, or the current traverse could be dismantled, cleaned, lubricated, and recalibrated to ensure its operation in no way inhibits displacement data accuracy. The control/driver outputs data accurate to +/- 0.005mm, but other devices may produce more precise data.

Tip loads could be designed differently for use in both static and vibration testing. Hanging weights from the tip of the current beam was a viable method for static loading, but vibration testing requires a load to the slipped around the tip of the beam. Changing

the beam's mass along its Y-axis disrupts its natural inertia, and vibrometer data cannot be produced for the tip of the beam.

5.2 Implications

Princeton beam displacement data were referenced for the past thirty years to validate computer models for homogeneous nonlinear beam deflection data verification. As the experiment's accuracy and precision are improved, future experimenters will have a more viable baseline to which to compare a computer model's results. Composite beams of different geometries can be tested in an improved manner. Hence, computer models will better match results for actual helicopter rotor blade deflections.

5.3 Conclusions

The Princeton beam experiments produced accurate data, but left a desire to improve precision. The observable trends include those regarding Z, X, and angular displacements in terms of varying tip loads and radial stations. The Y displacement data may be usable for helicopter beam design, but in terms of comparing data to the Princeton beam experiments, Y-axis deflections are unnecessary.

Horizontal, or X-axis, deflections tend to increase with decreasing pitch angles. As a helicopter's rotors move toward a more vertical position (tip view), they will deflect horizontally. As they tend toward a more horizontal position, the main beams will deflect more vertically. This seems to be the most important of the deflections, as a vertical beam will only serve to stall while a horizontal blade will produce lift at a favorable angle of attack. Even so, a pitch angle of thirty or sixty degrees may not be altogether implausible, and such situations must be examined as well.

The materials and dimensions for which beams are designed must be capable of withstanding the X, Y, Z, and angular deformations similar to those realized in this experiment. The current data obviously maintains a certain degree of precision, and such trials could be performed for differing materials and loads making nonhomogeneous blade models more precise, while procedural improvements can increase accuracy as well.

Appendix A: Corrected Data

The data presented in this appendix is a direct result of the actual experimental data tabulated in Appendix B. This data has been reproduced in terms of the elastic axis of the deflected beam. It was used for plot production and should be referenced as the main data recorded for the experiment. It should be noted that all tip loads recorded as whole numbers differ slightly from those in the tables. Initial pitch angles also are not precise whole numbers, and their actual values are recorded in the tables as well.

Table 2: Weight nomenclature

Recorded Load	Actual Load
(lb)	(lb)
0.00	0.00
0.50	0.49
1.00	1.01
1.50	1.50
2.00	2.01
2.50	2.51
3.00	3.00
3.50	3.51
4.00	4.02

Table 3: Corrected Data (0 deg)

Tip Load	Radial Station	Angle (arctan)		Elastic Axis Coordinates Space-Fixed Axes		
P, lb	r/R, N, D	Degrees	Δ angle	X, mm	Y, mm	Z, mm
0	1.00	0.000	0.000	-18.82	506.40	4.42
0	0.75	0.000	0.000	-11.06	379.66	4.74
0	0.50	0.000	0.000	-5.13	252.73	5.18
0	0.25	0.000	0.000	-0.84	125.84	5.70
0	0.00	0.000	0.000	0.00	0.00	0.00
1	1.00	0.000	0.000	-20.01	506.40	10.28
1	0.75	0.000	0.000	-12.07	379.66	8.45
1	0.50	0.000	0.000	-5.50	252.73	7.09
1	0.25	0.000	0.000	-0.87	125.84	6.06
1	0.00	0.000	0.000	0.00	0.00	0.00
2	1.00	0.000	0.000	-23.06	505.94	15.69
2	0.75	0.000	0.000	-13.28	379.66	12.11
2	0.50	0.000	0.000	-5.94	252.73	9.08
2	0.25	0.000	0.000	-1.19	125.84	6.87
2	0.00	0.000	0.000	0.00	0.00	0.00
3	1.00	0.000	0.000	-25.31	505.94	21.53
3	0.75	0.000	0.000	-15.05	379.66	15.73
3	0.50	0.000	0.000	-6.34	252.73	10.67
3	0.25	0.000	0.000	-1.18	125.84	7.45
3	0.00	0.000	0.000	0.00	0.00	0.00
4	1.00	0.000	0.000	-28.70	505.78	27.50
4	0.75	0.000	0.000	-16.77	379.35	19.55
4	0.50	0.000	0.000	-7.52	252.73	12.76
4	0.25	0.000	0.000	-1.63	125.84	8.03
4	0.00	0.000	0.000	0.00	0.00	0.00

Table 4: Corrected Data (15 deg)

Tip Load	Radial Station	Angle (arctan)		Elastic Axis Coordinates Space-Fixed Axes		
P, lb	r/R, N, D	Degrees	Δ angle	X, mm	Y, mm	Z, mm
0	1.00	14.036	0.046	-20.77	506.11	3.80
0	0.75	12.839	1.151	-13.72	380.11	1.67
0	0.50	12.947	1.044	-7.61	253.36	1.57
0	0.25	13.834	0.156	-2.94	126.62	0.70
0	0.00	13.990	0.000	0.00	0.00	0.00
1	1.00	12.038	1.952	-1.96	506.61	11.49
1	0.75	12.641	1.349	-1.26	380.09	8.30
1	0.50	12.954	1.036	-1.28	253.23	4.73
1	0.25	13.864	0.126	-1.13	126.52	1.61
1	0.00	13.990	0.000	0.00	0.00	0.00
2	1.00	10.265	3.725	17.60	506.62	23.28
2	0.75	13.136	0.854	11.51	379.66	14.87
2	0.50	13.581	0.409	4.92	253.55	8.13
2	0.25	13.731	0.259	0.59	126.52	2.83
2	0.00	13.990	0.000	0.00	0.00	0.00
3	1.00	13.876	0.114	40.21	503.87	33.28
3	0.75	14.128	0.138	23.71	379.14	21.81
3	0.50	14.141	0.151	11.26	253.48	11.44
3	0.25	14.820	0.830	2.45	126.54	3.53
3	0.00	13.990	0.000	0.00	0.00	0.00
4	1.00	17.007	3.017	62.93	500.08	45.63
4	0.75	15.475	1.484	40.57	377.20	30.01
4	0.50	15.888	1.897	20.25	252.70	15.47
4	0.25	15.699	1.709	5.88	126.73	4.63
4	0.00	13.990	0.000	0.00	0.00	0.00

Table 5: Corrected Data (-15 deg)

Tip Load	Radial Station	Angle		Elastic Axis Coordinates		
		(arctan)		Space-Fixed Axes		
P, lb	r/R, N, D	Degrees	Δ angle	X, mm	Y, mm	Z, mm
0	1.00	-17.312	1.742	-20.25	506.13	2.96
0	0.75	-16.826	1.256	-12.63	379.82	1.55
0	0.50	-16.241	0.672	-6.73	252.62	0.43
0	0.25	-15.504	0.066	-2.46	125.58	-0.21
0	0.00	-15.570	0.000	0.00	0.00	0.00
1	1.00	-17.838	2.268	-42.33	504.45	14.68
1	0.75	-17.110	1.540	-26.66	378.74	8.90
1	0.50	-16.533	0.964	-13.60	252.37	4.28
1	0.25	-16.173	0.603	-4.32	125.55	1.26
1	0.00	-15.570	0.000	0.00	0.00	0.00
2	1.00	-14.392	1.178	-64.81	500.90	29.02
2	0.75	-17.786	2.216	-40.53	376.99	16.69
2	0.50	-17.482	1.912	-20.57	251.71	8.26
2	0.25	-16.704	1.134	-6.61	125.55	2.22
2	0.00	-15.570	0.000	0.00	0.00	0.00
3	1.00	-20.414	4.845	-87.77	495.69	41.13
3	0.75	-19.419	3.850	-55.51	374.08	25.65
3	0.50	-18.895	3.325	-28.04	250.94	12.38
3	0.25	-17.863	2.293	-8.63	125.45	3.42
3	0.00	-15.570	0.000	0.00	0.00	0.00
4	1.00	-21.522	5.952	-111.75	487.49	56.56
4	0.75	-21.543	5.974	-70.52	369.78	35.43
4	0.50	-20.798	5.228	-35.39	249.23	16.92
4	0.25	-19.283	3.714	-10.55	125.14	4.73
4	0.00	-15.570	0.000	0.00	0.00	0.00

Table 6: Corrected Data (30 deg)

Tip Load	Radial Station	Angle (arctan)		Elastic Axis Coordinates Space-Fixed Axes		
P, lb	r/R, N, D	Degrees	Δ angle	X, mm	Y, mm	Z, mm
0	1.00	28.968	1.450	-19.25	505.57	-0.42
0	0.75	29.131	1.287	-13.62	379.70	1.15
0	0.50	29.918	0.501	-7.82	253.21	1.57
0	0.25	30.803	0.385	-3.28	126.15	1.02
0	0.00	30.418	0.000	0.00	0.00	0.00
1	1.00	28.586	1.832	16.41	505.89	26.90
1	0.75	29.244	1.175	9.96	379.80	18.63
1	0.50	29.557	0.861	4.13	253.62	10.19
1	0.25	29.920	0.498	0.09	126.74	3.67
1	0.00	30.418	0.000	0.00	0.00	0.00
2	1.00	30.996	0.577	51.89	501.03	54.43
2	0.75	30.655	0.237	32.15	377.33	35.69
2	0.50	30.767	0.348	15.22	252.60	18.87
2	0.25	30.727	0.309	3.25	126.71	6.26
2	0.00	30.418	0.000	0.00	0.00	0.00
3	1.00	32.437	2.018	85.16	491.39	81.23
3	0.75	32.682	2.264	54.14	372.07	53.28
3	0.50	32.404	1.985	26.42	250.74	27.47
3	0.25	32.082	1.664	6.54	126.48	8.58
3	0.00	30.418	0.000	0.00	0.00	0.00
4	1.00	36.091	5.673	117.61	476.57	110.56
4	0.75	36.002	5.584	74.96	363.81	71.93
4	0.50	35.250	4.831	37.03	247.76	36.68
4	0.25	33.842	3.424	9.58	126.32	11.10
4	0.00	30.418	0.000	0.00	0.00	0.00

Table 7: Corrected Data (-30 deg)

Tip Load	Radial Station	Angle (arctan)		Elastic Axis Coordinates Space-Fixed Axes		
P, lb	r/R, N, D	Degrees	Δ angle	X, mm	Y, mm	Z, mm
0	1.00	-32.267	2.497	-15.58	506.05	7.81
0	0.75	-30.762	0.992	-9.37	379.62	4.38
0	0.50	-33.309	3.540	-4.26	252.71	0.79
0	0.25	-30.166	0.397	-1.37	125.24	0.64
0	0.00	-29.770	0.000	0.00	0.00	0.00
1	1.00	-32.804	3.034	-51.26	501.81	35.09
1	0.75	-31.122	1.352	-32.22	377.35	21.78
1	0.50	-31.822	2.052	-15.58	251.94	10.71
1	0.25	-31.055	1.285	-4.51	125.24	3.13
1	0.00	-29.770	0.000	0.00	0.00	0.00
2	1.00	-33.221	3.451	-85.03	492.93	69.55
2	0.75	-31.450	1.680	-52.26	372.95	38.42
2	0.50	-32.920	3.150	-25.60	250.36	18.89
2	0.25	-31.302	1.532	-7.59	125.14	5.53
2	0.00	-29.770	0.000	0.00	0.00	0.00
3	1.00	-37.658	7.888	-119.13	479.37	90.41
3	0.75	-36.264	6.494	-70.35	366.81	54.75
3	0.50	-36.129	6.359	-37.55	247.51	28.45
3	0.25	-34.506	4.736	-10.42	124.93	7.92
3	0.00	-29.770	0.000	0.00	0.00	0.00
4	1.00	-39.218	9.448	-145.78	462.78	118.10
4	0.75	-38.860	9.090	-90.84	356.78	73.91
4	0.50	-37.370	7.600	-45.90	244.50	36.56
4	0.25	-35.103	5.333	-13.13	124.40	10.33
4	0.00	-29.770	0.000	0.00	0.00	0.00

Table 8: Corrected Data (45 deg)

Tip Load	Radial Station	Angle		Elastic Axis Coordinates		
		(arctan)		Space-Fixed Axes		
P, lb	r/R, N, D	Degrees	Δ angle	X, mm	Y, mm	Z, mm
0	1.00	43.454	1.721	-13.73	506.37	-3.84
0	0.75	43.829	1.346	-8.67	380.57	-1.35
0	0.50	44.156	1.019	-4.82	254.18	0.18
0	0.25	44.897	0.278	-1.89	127.05	0.47
0	0.00	45.175	0.000	0.00	0.00	0.00
1	1.00	43.771	1.404	44.79	504.36	42.63
1	0.75	44.575	0.600	17.66	379.51	28.56
1	0.50	44.479	0.696	8.55	253.64	15.01
1	0.25	45.142	0.033	2.06	127.27	4.63
1	0.00	45.175	0.000	0.00	0.00	0.00
2	1.00	44.547	0.628	65.19	493.86	87.93
2	0.75	45.036	0.139	41.71	373.36	57.57
2	0.50	45.295	0.120	20.48	251.35	29.88
2	0.25	52.779	7.604	5.38	126.93	10.03
2	0.00	45.175	0.000	0.00	0.00	0.00
3	1.00	50.464	5.289	93.63	476.69	129.37
3	0.75	47.087	1.912	59.78	363.83	84.36
3	0.50	47.598	2.423	29.55	247.68	43.32
3	0.25	46.664	1.489	7.69	125.98	12.81
3	0.00	45.175	0.000	0.00	0.00	0.00

Table 9: Corrected Data (-45 deg)

Tip Load	Radial Station	Angle		Elastic Axis Coordinates		
		(arctan)		Space-Fixed Axes		
P, lb	r/R, N, D	Degrees	Δ angle	X, mm	Y, mm	Z, mm
0	1.00	-47.008	1.769	-15.65	505.65	12.46
0	0.75	-46.150	0.910	-9.83	379.02	7.25
0	0.50	-45.600	0.360	-5.27	252.12	3.38
0	0.25	-46.064	0.824	-1.85	125.06	1.01
0	0.00	-45.240	0.000	0.00	0.00	0.00
1	1.00	-47.868	2.628	-55.94	497.99	59.93
1	0.75	-47.577	2.338	-35.56	375.10	37.58
1	0.50	-47.254	2.014	-18.07	250.72	18.66
1	0.25	-46.237	0.997	-5.57	124.82	5.27
1	0.00	-45.240	0.000	0.00	0.00	0.00
2	1.00	-42.091	3.148	-90.72	483.02	102.54
2	0.75	-48.722	3.483	-57.92	366.68	65.60
2	0.50	-48.118	2.879	-29.54	247.60	32.68
2	0.25	-47.280	2.040	-8.87	124.39	9.29
2	0.00	-45.240	0.000	0.00	0.00	0.00
3	1.00	-51.386	6.147	-119.12	462.42	144.25
3	0.75	-50.908	5.669	-76.83	355.54	91.84
3	0.50	-50.081	4.841	-39.48	243.34	45.89
3	0.25	-48.548	3.308	-11.94	123.54	12.88
3	0.00	-45.240	0.000	0.00	0.00	0.00

Table 10: Corrected Data (60 deg)

Tip Load	Radial Station	Angle		Elastic Axis Coordinates		
		(arctan)		Space-Fixed Axes		
P, lb	r/R, N, D	Degrees	Δ angle	X, mm	Y, mm	Z, mm
0	1.00	60.021	2.248	-16.49	506.72	-6.74
0	0.75	60.854	1.415	-10.67	380.21	-3.51
0	0.50	61.035	1.234	-6.64	253.76	-1.09
0	0.25	61.561	0.708	-2.96	126.87	-0.07
0	0.00	62.269	0.000	0.00	0.00	0.00
0.5	1.00	60.335	1.934	3.48	506.38	27.33
0.5	0.75	60.471	1.798	0.06	380.21	18.62
0.5	0.50	61.165	1.103	-1.16	253.73	10.06
0.5	0.25	61.482	0.787	-1.40	127.05	3.19
0.5	0.00	62.269	0.000	0.00	0.00	0.00
1	1.00	62.004	0.264	34.16	502.40	62.10
1	0.75	60.731	1.538	26.48	378.07	40.97
1	0.50	61.071	1.198	10.72	253.32	21.28
1	0.25	61.605	0.664	0.32	126.95	6.35
1	0.00	62.269	0.000	0.00	0.00	0.00
1.5	1.00	61.059	1.210	40.30	495.97	95.17
1.5	0.75	61.183	1.086	28.78	374.42	62.01
1.5	0.50	61.237	1.032	9.91	251.63	31.82
1.5	0.25	62.015	0.254	1.66	127.00	9.63
1.5	0.00	62.269	0.000	0.00	0.00	0.00
2	1.00	61.358	0.911	49.33	486.56	125.86
2	0.75	60.777	1.492	30.92	368.99	81.93
2	0.50	61.663	0.606	14.61	249.75	42.19
2	0.25	62.324	0.055	2.95	126.50	12.65
2	0.00	62.269	0.000	0.00	0.00	0.00

Table 11: Corrected Data (-60 deg)

Tip Load	Radial Station	Angle (arctan)		Elastic Axis Coordinates Space-Fixed Axes		
P, lb	r/R, N, D	Degrees	Δ angle	X, mm	Y, mm	Z, mm
0	1.00	-63.302	1.467	-10.87	505.51	16.35
0	0.75	-62.364	0.529	-6.93	378.83	9.70
0	0.50	-62.709	0.874	-3.57	252.03	4.80
0	0.25	-62.140	0.305	-1.31	124.81	1.41
0	0.00	-61.835	0.000	0.00	0.00	0.00
0.5	1.00	-63.390	1.555	-27.61	501.90	50.31
0.5	0.75	-63.111	1.275	-17.55	376.89	31.42
0.5	0.50	-62.517	0.682	-9.03	251.45	15.58
0.5	0.25	-62.311	0.476	-2.89	124.84	4.46
0.5	0.00	-61.835	0.000	0.00	0.00	0.00
1	1.00	-63.749	1.913	-43.65	494.99	84.22
1	0.75	-63.435	1.600	-27.85	373.46	53.16
1	0.50	-62.644	0.809	-14.30	250.19	26.48
1	0.25	-62.477	0.642	-4.30	124.57	7.61
1	0.00	-61.835	0.000	0.00	0.00	0.00
1.5	1.00	-65.105	3.269	-57.32	486.44	113.80
1.5	0.75	-63.760	1.925	-36.81	368.63	72.03
1.5	0.50	-63.701	1.865	-18.72	248.14	36.07
1.5	0.25	-63.062	1.227	-5.59	124.27	10.37
1.5	0.00	-61.835	0.000	0.00	0.00	0.00
2	1.00	-64.767	2.931	-70.50	474.79	143.86
2	0.75	-64.654	2.819	-45.18	362.04	91.56
2	0.50	-64.195	2.359	-23.28	245.84	46.00
2	0.25	-63.130	1.294	-7.07	124.07	13.22
2	0.00	-61.835	0.000	0.00	0.00	0.00

Table 12: Corrected Data (75 deg)

Tip Load	Radial Station	Angle		Elastic Axis Coordinates		
		(arctan)		Space-Fixed Axes		
P, lb	r/R, N, D	Degrees	Δ angle	X, mm	Y, mm	Z, mm
0	1.00	75.403	1.805	-12.10	506.36	-9.21
0	0.75	75.342	1.867	-8.58	380.09	-4.70
0	0.50	76.271	0.938	-5.33	253.75	-1.85
0	0.25	76.486	0.723	-2.58	126.98	-0.40
0	0.00	77.209	0.000	0.00	0.00	0.00
0.5	1.00	79.830	2.621	-0.21	506.30	32.69
0.5	0.75	79.421	2.213	-0.17	380.00	21.89
0.5	0.50	75.998	1.211	-2.38	254.00	11.50
0.5	0.25	76.581	0.628	-1.71	127.03	3.45
0.5	0.00	77.209	0.000	0.00	0.00	0.00
1	1.00	74.997	2.212	6.21	501.31	73.93
1	0.75	75.140	2.068	2.88	377.61	48.39
1	0.50	75.895	1.313	0.21	252.86	24.83
1	0.25	75.769	1.440	-1.11	127.18	7.22
1	0.00	77.209	0.000	0.00	0.00	0.00
1.5	1.00	74.568	2.641	14.95	492.94	112.09
1.5	0.75	75.244	1.965	8.42	373.02	72.97
1.5	0.50	76.081	1.128	3.08	251.03	37.20
1.5	0.25	76.861	0.347	-0.19	126.97	10.94
1.5	0.00	77.209	0.000	0.00	0.00	0.00

Table 13: Corrected Data (-75 deg)

Tip Load	Radial Station	Angle		Elastic Axis Coordinates		
		(arctan)		Space-Fixed Axes		
P, lb	r/R, N, D	Degrees	Δ angle	X, mm	Y, mm	Z, mm
0	1.00	-77.535	1.031	-6.27	506.28	18.56
0	0.75	-76.710	1.855	-4.04	379.64	11.26
0	0.50	-76.291	2.274	-2.48	252.80	5.56
0	0.25	-75.455	3.110	-1.16	125.55	1.87
0	0.00	-78.565	0.000	0.00	0.00	0.00
0.5	1.00	-77.674	0.891	-15.51	502.20	59.08
0.5	0.75	-78.094	0.471	-9.93	377.41	36.96
0.5	0.50	-76.928	1.637	-5.47	252.02	18.51
0.5	0.25	-76.268	2.297	-1.99	125.28	5.48
0.5	0.00	-78.565	0.000	0.00	0.00	0.00
1	1.00	-77.551	1.014	-24.39	494.49	98.84
1	0.75	-77.086	1.480	-15.76	373.35	62.42
1	0.50	-77.097	1.469	-8.25	250.44	31.33
1	0.25	-76.605	1.960	-2.79	125.16	9.17
1	0.00	-78.565	0.000	0.00	0.00	0.00
1.5	1.00	-78.500	0.065	-31.57	484.38	132.20
1.5	0.75	-77.565	1.001	-20.40	367.69	83.90
1.5	0.50	-76.798	1.767	-10.62	248.38	42.31
1.5	0.25	-77.179	1.387	-3.42	124.82	12.26
1.5	0.00	-78.565	0.000	0.00	0.00	0.00

Table 14: Corrected Data (90 deg)

Tip Load	Radial Station	Angle (arctan)		Elastic Axis Coordinates Space-Fixed Axes		
P, lb	r/R, N, D	Degrees	Δ angle	X, mm	Y, mm	Z, mm
0	1.00	88.491	0.139	-8.71	506.18	-10.50
0	0.75	89.806	1.454	-6.36	380.42	-5.76
0	0.50	89.902	1.549	-4.09	253.63	-2.53
0	0.25	88.927	0.575	-2.22	127.08	-0.70
0	0.00	88.352	0.000	0.00	0.00	0.00
0.5	1.00	88.441	0.089	-8.42	505.60	33.08
0.5	0.75	89.803	1.451	-6.84	379.98	22.18
0.5	0.50	89.449	1.097	-4.52	253.63	11.53
0.5	0.25	88.879	0.526	-2.22	127.08	3.33
0.5	0.00	88.352	0.000	0.00	0.00	0.00
1	1.00	86.333	2.019	-9.22	500.22	78.26
1	0.75	87.074	1.278	-7.31	376.95	50.12
1	0.50	88.192	0.160	-4.77	252.56	24.87
1	0.25	88.586	0.234	-2.23	127.08	7.49
1	0.00	88.352	0.000	0.00	0.00	0.00
1.5	1.00	85.632	2.720	-9.80	491.85	116.97
1.5	0.75	88.889	0.537	-7.67	372.08	75.78
1.5	0.50	89.426	1.074	-5.27	250.92	38.93
1.5	0.25	89.561	1.209	-2.20	127.08	11.06
1.5	0.00	88.352	0.000	0.00	0.00	0.00

Table 15: Corrected Data (-90 deg)

Tip Load	Radial Station	Angle (arctan)		Elastic Axis Coordinates Space-Fixed Axes		
P, lb	r/R, N, D	Degrees	Δ angle	X, mm	Y, mm	Z, mm
0	1.00	-87.745	2.158	-0.51	505.89	18.70
0	0.75	-89.033	0.870	-0.23	379.12	11.24
0	0.50	-88.508	1.395	-0.27	252.13	5.45
0	0.25	-89.288	0.615	-0.16	125.02	1.59
0	0.00	-89.903	0.000	0.00	0.00	0.00
0.5	1.00	-88.062	1.841	-0.01	501.77	61.09
0.5	0.75	-88.490	1.413	-0.03	377.03	38.22
0.5	0.50	-89.175	0.728	-0.21	251.57	18.96
0.5	0.25	-89.421	0.481	-0.16	124.99	5.50
0.5	0.00	-89.903	0.000	0.00	0.00	0.00
1	1.00	-87.256	2.647	0.26	493.25	103.61
1	0.75	-88.422	1.481	-0.14	372.62	65.55
1	0.50	-88.566	1.337	-0.14	249.87	32.77
1	0.25	-89.421	0.481	-0.16	124.87	9.50
1	0.00	-89.903	0.000	0.00	0.00	0.00
1.5	1.00	-87.585	2.318	0.92	482.99	139.22
1.5	0.75	-88.954	0.949	0.22	366.76	88.68
1.5	0.50	-89.074	0.829	-0.08	247.83	44.60
1.5	0.25	-89.186	0.717	-0.21	124.34	12.80
1.5	0.00	-89.903	0.000	0.00	0.00	0.00

Table 16: Corrected Data (180 deg)

Tip Load	Radial Station	Angle (arctan)		Elastic Axis Coordinates Space-Fixed Axes		
P, lb	r/R, N, D	Degrees	Δ angle	X, mm	Y, mm	Z, mm
0	1.00	180.000	0.000	17.17	507.95	9.30
0	0.75	180.000	0.000	9.41	380.31	7.80
0	0.50	180.000	0.000	5.20	253.50	8.05
0	0.25	180.000	0.000	2.50	126.70	7.11
0	0.00	180.000	0.000	0.00	0.00	0.00
3	1.00	180.000	0.000	10.89	507.67	26.70
3	0.75	180.000	0.000	5.92	379.00	19.85
3	0.50	180.000	0.000	3.34	253.21	13.63
3	0.25	180.000	0.000	2.07	126.12	9.01
3	0.00	180.000	0.000	0.00	0.00	0.00

Appendix B: Original Data

The raw data tabulated in this section are the actual data taken from the driver/controller prior to any negative, positive, or elastic axis corrections. They directly relate to the data recorded in Appendix A.

Table 17: Original Data (0 deg)

Tip Load	Radial Station	Deflection		
		Space-Fixed Axes		
P, lb	r/R, N, D	X, mm	Y, mm	Z, mm
0	1.00	9979.59	9493.60	9998.07
0	0.75	9987.35	9620.34	9998.39
0	0.50	9993.28	9747.27	9998.83
0	0.25	9997.57	9874.16	9999.35
0	0.00	0.00	0.00	0.00
1	1.00	9978.40	9493.60	3.93
1	0.75	9986.34	9620.34	2.10
1	0.50	9992.91	9747.27	0.74
1	0.25	9997.54	9874.16	9999.71
1	0.00	0.00	0.00	0.00
2	1.00	9975.35	9494.06	9.34
2	0.75	9985.13	9620.34	5.76
2	0.50	9992.47	9747.27	2.73
2	0.25	9997.22	9874.16	0.52
2	0.00	0.00	0.00	0.00
3	1.00	9973.10	9494.06	15.18
3	0.75	9983.36	9620.34	9.38
3	0.50	9992.07	9747.27	4.32
3	0.25	9997.23	9874.16	1.10
3	0.00	0.00	0.00	0.00
4	1.00	9969.71	9494.22	21.15
4	0.75	9981.64	9620.65	13.20
4	0.50	9990.89	9747.27	6.41
4	0.25	9996.78	9874.16	1.68
4	0.00	0.00	0.00	0.00

Table 18: Original Data (15 deg)

Tip Load	Radial Station	Deflection Data					
		Space-Fixed Axes (left side)			Space-Fixed Axes (right side)		
P, lb	r/R, N, D	X, mm	Y, mm	Z, mm	X, mm	Y, mm	Z, mm
0	1.00	21.53	506.34	6.84	22.93	505.88	12.44
0	0.75	13.85	380.11	1.71	16.48	380.11	13.25
0	0.50	7.76	253.36	1.73	10.36	253.36	13.04
0	0.25	2.91	126.62	0.53	5.87	126.62	12.55
0	0.00	0.00	0.00	0.00	2.91	0.00	11.68
1	1.00	2.23	506.61	11.77	4.58	506.61	22.79
1	0.75	1.38	380.09	8.17	4.04	380.09	20.03
1	0.50	1.42	253.23	4.85	4.04	253.23	16.24
1	0.25	1.13	126.52	1.57	4.03	126.52	13.32
1	0.00	0.00	0.00	0.00	2.91	0.00	11.68
2	1.00	9982.56	506.62	21.98	9985.11	506.62	36.06
2	0.75	9988.59	379.66	14.90	9991.29	379.66	26.47
2	0.50	9995.10	253.55	8.02	9997.97	253.55	19.90
2	0.25	9999.40	126.52	2.69	2.32	126.52	14.64
2	0.00	0.00	0.00	0.00	2.91	0.00	11.68
3	1.00	9959.89	504.26	33.65	9962.59	503.47	44.58
3	0.75	9976.26	379.14	21.75	9979.23	379.14	33.55
3	0.50	9988.74	253.48	11.51	9991.65	253.48	23.06
3	0.25	9997.45	126.54	3.48	0.58	126.54	15.31
3	0.00	0.00	0.00	0.00	2.91	0.00	11.68
4	1.00	9936.80	500.91	45.85	9940.29	499.25	57.26
4	0.75	9959.25	377.20	29.93	9962.55	377.20	41.85
4	0.50	9979.54	252.70	15.48	9982.89	252.70	27.25
4	0.25	9993.95	126.73	4.68	9997.23	126.73	16.35
4	0.00	0.00	0.00	0.00	2.91	0.00	11.68

Table 19: Original Data (-15 deg)

Tip Load	Radial Station	Deflection Data					
		Space-Fixed Axes (left side)			Space-Fixed Axes (right side)		
P, lb	r/R, N, D	X, mm	Y, mm	Z, mm	X, mm	Y, mm	Z, mm
0	1.00	9979.57	9493.87	2.99	9983.17	9493.87	14.54
0	0.75	9987.30	9620.18	1.76	9990.69	9620.18	12.97
0	0.50	9993.22	9747.38	0.51	9996.57	9747.38	12.01
0	0.25	9997.58	9874.42	9999.89	0.77	9874.42	11.39
0	0.00	0.00	0.00	0.00	3.26	0.00	11.70
1	1.00	9957.56	9495.55	15.12	9961.00	9495.55	25.81
1	0.75	9973.23	9621.26	9.09	9976.69	9621.26	20.33
1	0.50	9986.33	9747.63	4.39	9989.72	9747.63	15.81
1	0.25	9995.67	9874.45	1.44	9998.95	9874.45	12.75
1	0.00	0.00	0.00	0.00	3.26	0.00	11.70
2	1.00	9934.98	9499.10	27.71	9938.67	9499.10	42.09
2	0.75	9959.29	9623.01	16.90	9962.87	9623.01	28.06
2	0.50	9979.27	9748.29	8.44	9982.81	9748.29	19.68
2	0.25	9993.31	9874.45	2.37	9996.71	9874.45	13.70
2	0.00	0.00	0.00	0.00	3.26	0.00	11.70
3	1.00	9911.92	9504.31	41.75	9915.72	9504.31	51.96
3	0.75	9944.07	9625.92	25.67	9948.11	9625.92	37.13
3	0.50	9971.71	9749.06	12.74	9975.41	9749.06	23.55
3	0.25	9991.14	9874.55	3.48	9994.83	9874.55	14.93
3	0.00	0.00	0.00	0.00	3.26	0.00	11.70
4	1.00	9887.80	9512.51	57.12	9891.85	9512.51	67.39
4	0.75	9928.94	9630.22	35.75	9933.18	9630.22	46.49
4	0.50	9964.12	9750.77	17.18	9968.26	9750.77	28.08
4	0.25	9989.11	9874.86	4.94	9992.99	9874.86	16.03
4	0.00	0.00	0.00	0.00	3.26	0.00	11.70

Table 20: Original Data (30 deg)

Tip Load	Radial Station	Deflection Data					
		Space-Fixed Axes (left side)			Space-Fixed Axes (right side)		
P, lb	r/R, N, D	X, mm	Y, mm	Z, mm	X, mm	Y, mm	Z, mm
0	1.00	19.54	505.57	9999.79	24.86	505.57	9.40
0	0.75	13.75	379.70	1.11	19.39	379.70	11.23
0	0.50	7.80	253.21	1.44	13.75	253.21	11.78
0	0.25	3.28	126.15	1.09	9.23	126.15	15.36
0	0.00	0.00	0.00	0.00	5.93	0.00	10.10
1	1.00	9983.83	505.89	26.95	9989.23	505.89	36.86
1	0.75	9990.04	379.93	18.39	9995.93	379.66	28.91
1	0.50	9995.93	253.62	10.11	1.72	253.62	20.32
1	0.25	9999.84	126.82	3.44	5.90	126.65	13.97
1	0.00	0.00	0.00	0.00	5.93	0.00	10.10
2	1.00	9948.71	501.30	53.55	9953.45	500.75	63.44
2	0.75	9967.81	377.63	35.68	9973.82	377.02	45.82
2	0.50	9984.81	252.80	19.00	9990.68	252.40	28.86
2	0.25	9996.74	126.71	6.31	2.69	126.71	16.32
2	0.00	0.00	0.00	0.00	5.93	0.00	10.10
3	1.00	9914.77	491.85	81.51	9920.89	490.92	91.14
3	0.75	9945.71	372.39	53.47	9952.01	371.74	63.29
3	0.50	9973.43	250.93	27.61	9979.72	250.54	37.52
3	0.25	9993.30	126.55	8.64	9999.60	126.40	18.69
3	0.00	0.00	0.00	0.00	5.93	0.00	10.10
4	1.00	9882.15	477.13	111.22	9888.74	476.01	120.26
4	0.75	9924.67	364.32	72.41	9931.50	363.30	81.81
4	0.50	9962.54	247.99	36.93	9969.48	247.52	46.75
4	0.25	9990.24	126.52	11.47	9996.63	126.11	21.00
4	0.00	0.00	0.00	0.00	5.93	0.00	10.10

Table 21: Original Data (-30 deg)

Tip Load	Radial Station	Deflection Data					
		Space-Fixed Axes (left side)			Space-Fixed Axes (right side)		
P, lb	r/R, N, D	X, mm	Y, mm	Z, mm	X, mm	Y, mm	Z, mm
0	1.00	9984.04	9493.89	7.68	9990.36	9494.00	17.69
0	0.75	9990.45	9620.38	4.27	9996.42	9620.38	14.30
0	0.50	9995.30	9747.29	2.14	1.72	9747.29	10.52
0	0.25	9998.56	9874.85	0.61	4.32	9874.68	10.52
0	0.00	0.00	0.00	0.00	5.64	0.00	9.86
1	1.00	9948.41	9498.07	35.12	9954.63	9498.31	44.77
1	0.75	9967.53	9622.65	21.62	9973.64	9622.65	31.74
1	0.50	9984.16	9748.06	10.68	9990.26	9748.06	20.51
1	0.25	9995.23	9874.85	2.94	1.36	9874.68	13.12
1	0.00	0.00	0.00	0.00	5.64	0.00	9.86
2	1.00	9914.50	9507.07	62.44	9920.99	9507.07	79.35
2	0.75	9947.43	9626.92	38.22	9953.65	9627.19	48.39
2	0.50	9973.98	9749.47	18.81	9980.37	9749.81	28.68
2	0.25	9992.11	9874.85	5.33	9998.30	9874.87	15.51
2	0.00	0.00	0.00	0.00	5.64	0.00	9.86
3	1.00	9880.10	9520.35	90.67	9887.03	9520.92	99.65
3	0.75	9928.85	9632.95	54.72	9935.90	9633.43	64.33
3	0.50	9961.75	9752.26	28.55	9968.59	9752.73	37.92
3	0.25	9988.97	9874.99	7.84	9995.70	9875.15	17.63
3	0.00	0.00	0.00	0.00	5.64	0.00	9.86
4	1.00	9853.34	9537.08	118.46	9860.44	9537.36	127.16
4	0.75	9908.19	9643.06	74.10	9915.49	9643.38	83.16
4	0.50	9953.33	9755.38	36.76	9960.28	9755.63	45.86
4	0.25	9986.22	9875.50	10.31	9993.01	9875.71	19.97
4	0.00	0.00	0.00	0.00	5.64	0.00	9.86

Table 22: Original Data (45 deg)

Tip Load	Radial Station	Deflection Data					
		Space-Fixed Axes (left side)			Space-Fixed Axes (right side)		
P, lb	r/R, N, D	X, mm	Y, mm	Z, mm	X, mm	Y, mm	Z, mm
0	1.00	13.75	506.37	9995.93	21.86	506.37	4.49
0	0.75	8.67	380.57	9998.46	16.82	380.57	6.95
0	0.50	4.73	254.18	9999.93	13.09	254.18	8.54
0	0.25	1.84	127.05	0.38	10.14	127.05	8.71
0	0.00	0.00	0.00	0.00	8.21	0.00	8.16
1	1.00	9955.30	504.47	42.52	9963.28	504.25	50.85
1	0.75	9982.42	379.81	28.56	9990.44	379.21	36.70
1	0.50	9991.45	253.64	14.91	9999.63	253.64	23.24
1	0.25	9998.00	127.27	4.69	6.08	127.27	12.73
1	0.00	0.00	0.00	0.00	8.21	0.00	8.16
2	1.00	9934.83	493.86	87.86	9942.98	493.86	96.14
2	0.75	9958.36	373.56	57.62	9966.43	373.15	65.68
2	0.50	9979.62	251.35	30.00	9987.63	251.35	37.93
2	0.25	9994.72	126.93	11.09	3.04	126.93	17.41
2	0.00	0.00	0.00	0.00	8.21	0.00	8.16
3	1.00	9906.17	477.58	129.91	9914.99	475.79	137.19
3	0.75	9940.17	364.07	84.58	9948.56	363.58	92.38
3	0.50	9970.28	247.95	43.50	9978.92	247.41	51.39
3	0.25	9992.10	125.98	12.82	0.78	125.98	21.01
3	0.00	0.00	0.00	0.00	8.21	0.00	8.16

Table 23: Original Data (-45 deg)

Tip Load	Radial Station	Deflection Data					
		Space-Fixed Axes (left side)			Space-Fixed Axes (right side)		
P, lb	r/R, N, D	X, mm	Y, mm	Z, mm	X, mm	Y, mm	Z, mm
0	1.00	9984.23	9494.35	12.60	9992.79	9494.35	20.58
0	0.75	9990.03	9620.98	7.25	9998.67	9620.98	15.55
0	0.50	9994.58	9747.88	3.28	3.27	9747.88	11.79
0	0.25	9998.08	9874.94	1.06	6.58	9874.94	9.25
0	0.00	0.00	0.00	0.00	8.40	0.00	8.33
1	1.00	9943.96	9501.94	60.20	9952.45	9502.09	67.88
1	0.75	9964.30	9624.82	37.78	9972.89	9624.98	45.63
1	0.50	9981.86	9749.17	18.88	9990.31	9749.40	26.69
1	0.25	9994.47	9875.18	5.45	2.75	9875.18	13.38
1	0.00	0.00	0.00	0.00	8.40	0.00	8.33
2	1.00	9909.15	9516.98	101.91	9917.93	9516.98	111.63
2	0.75	9941.79	9633.32	65.82	9950.63	9633.32	73.58
2	0.50	9970.25	9752.40	32.89	9978.96	9752.40	40.70
2	0.25	9990.98	9875.61	9.44	9999.60	9875.61	17.40
2	0.00	0.00	0.00	0.00	8.40	0.00	8.33
3	1.00	9880.41	9537.58	144.67	9889.50	9537.58	151.93
3	0.75	9922.67	9644.46	92.18	9931.84	9644.46	99.63
3	0.50	9960.15	9756.66	46.22	9969.09	9756.66	53.70
3	0.25	9987.87	9876.46	13.16	9996.52	9876.46	20.80
3	0.00	0.00	0.00	0.00	8.40	0.00	8.33

Table 24: Original Data (60 deg)

Tip Load	Radial Station	Deflection Data					
		Space-Fixed Axes (left side)			Space-Fixed Axes (right side)		
P, lb	r/R, N, D	X, mm	Y, mm	Z, mm	X, mm	Y, mm	Z, mm
0	1.00	15.54	506.72	9992.45	25.64	506.72	9999.43
0	0.75	10.76	380.21	9996.38	20.90	380.21	1.99
0	0.50	6.58	253.76	9998.73	16.95	253.76	4.47
0	0.25	2.93	126.87	9999.83	13.27	126.87	5.43
0	0.00	0.00	0.00	0.00	10.31	0.00	5.42
0.5	1.00	9996.60	506.58	27.15	6.66	506.18	32.88
0.5	0.75	9999.90	380.21	18.39	10.21	380.21	24.23
0.5	0.50	1.19	253.84	9.95	11.38	253.62	15.56
0.5	0.25	1.35	127.05	3.07	11.73	127.05	8.71
0.5	0.00	0.00	0.00	0.00	10.31	0.00	5.42
1	1.00	9965.77	502.75	62.03	9976.21	502.04	67.58
1	0.75	9973.55	378.15	40.81	9983.72	377.99	46.51
1	0.50	9989.19	253.32	21.09	9999.63	253.32	26.86
1	0.25	9999.58	127.09	6.22	10.05	126.81	11.88
1	0.00	0.00	0.00	0.00	10.31	0.00	5.42
1.5	1.00	9959.68	496.14	95.02	9969.97	495.79	100.71
1.5	0.75	9971.11	374.60	61.83	9981.58	374.23	67.59
1.5	0.50	9990.11	251.63	31.71	0.33	251.63	37.32
1.5	0.25	9998.23	127.00	9.54	8.75	127.00	15.13
1.5	0.00	0.00	0.00	0.00	10.31	0.00	5.42
2	1.00	9950.77	486.78	125.81	9960.84	486.33	131.31
2	0.75	9969.15	368.99	81.80	9979.25	368.99	87.45
2	0.50	9985.38	249.75	42.11	9995.69	249.75	47.67
2	0.25	9996.90	126.50	12.58	7.52	126.50	18.15
2	0.00	0.00	0.00	0.00	10.31	0.00	5.42

Table 25: Original Data (-60 deg)

Tip Load	Radial Station	Deflection Data					
		Space-Fixed Axes (left side)			Space-Fixed Axes (right side)		
P, lb	r/R, N, D	X, mm	Y, mm	Z, mm	X, mm	Y, mm	Z, mm
0	1.00	9989.09	9494.49	16.50	9999.41	9494.49	21.69
0	0.75	9992.91	9621.17	9.68	3.51	9621.17	15.23
0	0.50	9996.39	9747.97	4.88	6.74	9747.97	10.22
0	0.25	9998.59	9875.19	1.39	9.09	9875.19	6.94
0	0.00	0.00	0.00	0.00	10.31	0.00	5.52
0.5	1.00	9972.43	9498.10	50.51	9982.59	9498.10	55.60
0.5	0.75	9982.29	9623.11	31.48	9992.86	9623.11	36.84
0.5	0.50	9990.91	9748.55	15.63	1.31	9748.55	21.04
0.5	0.25	9997.00	9875.16	4.46	7.50	9875.16	9.97
0.5	0.00	0.00	0.00	0.00	10.31	0.00	5.52
1	1.00	9956.33	9505.01	84.43	9966.59	9505.01	89.49
1	0.75	9972.01	9626.54	53.27	9982.53	9626.54	58.53
1	0.50	9985.66	9749.81	26.55	9996.02	9749.81	31.91
1	0.25	9995.62	9875.43	7.64	6.06	9875.43	13.08
1	0.00	0.00	0.00	0.00	10.31	0.00	5.52
1.5	1.00	9942.46	9513.56	114.06	9953.04	9513.56	118.97
1.5	0.75	9963.00	9631.37	72.16	9973.59	9631.37	77.38
1.5	0.50	9981.20	9751.86	36.24	9991.58	9751.86	41.37
1.5	0.25	9994.33	9875.73	10.47	4.74	9875.73	15.76
1.5	0.00	0.00	0.00	0.00	10.31	0.00	5.52
2	1.00	9929.45	9525.21	144.16	9939.72	9525.21	149.00
2	0.75	9954.68	9637.96	91.81	9965.13	9637.96	96.76
2	0.50	9976.50	9754.16	46.16	9987.13	9754.16	51.30
2	0.25	9992.81	9875.93	13.31	3.29	9875.93	18.62
2	0.00	0.00	0.00	0.00	10.31	0.00	5.52

Table 26: Original Data (75 deg)

Tip Load	Radial Station	Deflection Data					
		Space-Fixed Axes (left side)			Space-Fixed Axes (right side)		
P, lb	r/R, N, D	X, mm	Y, mm	Z, mm	X, mm	Y, mm	Z, mm
0	1.00	12.06	506.36	9990.59	23.58	506.36	9993.59
0	0.75	8.68	380.09	9995.13	19.92	380.09	9998.07
0	0.50	5.14	253.75	9998.00	17.01	253.75	0.90
0	0.25	2.51	126.98	9999.51	14.16	126.98	2.31
0	0.00	0.00	0.00	0.00	11.54	0.00	2.62
0.5	1.00	9998.00	506.57	32.57	14.11	506.02	35.46
0.5	0.75	9998.00	380.00	21.72	14.01	380.00	24.71
0.5	0.50	2.22	254.00	11.33	14.01	254.00	14.27
0.5	0.25	1.66	127.03	3.37	13.27	127.03	6.14
0.5	0.00	0.00	0.00	0.00	11.54	0.00	2.62
1	1.00	9993.81	501.31	73.70	5.19	501.31	76.75
1	0.75	9997.12	377.61	48.17	8.54	377.61	51.20
1	0.50	9999.61	252.86	24.65	11.43	252.86	27.62
1	0.25	0.97	127.18	7.03	12.72	127.18	10.01
1	0.00	0.00	0.00	0.00	11.54	0.00	2.62
1.5	1.00	9985.13	492.94	111.83	9996.36	492.94	114.93
1.5	0.75	9991.60	373.02	72.77	2.99	373.02	75.77
1.5	0.50	9996.89	251.03	37.07	8.43	251.03	39.93
1.5	0.25	0.00	126.97	10.86	11.91	126.97	13.64
1.5	0.00	0.00	0.00	0.00	11.54	0.00	2.62

Table 27: Original Data (-75 deg)

Tip Load	Radial Station	Deflection Data					
		Space-Fixed Axes (left side)			Space-Fixed Axes (right side)		
P, lb	r/R, N, D	X, mm	Y, mm	Z, mm	X, mm	Y, mm	Z, mm
0	1.00	9993.75	9493.72	18.46	5.24	9493.72	21.00
0	0.75	9995.95	9620.36	11.06	7.55	9620.36	13.80
0	0.50	9997.54	9747.20	5.32	9.10	9747.20	8.14
0	0.25	9998.84	9874.45	1.54	10.48	9874.45	4.56
0	0.00	0.00	0.00	0.00	11.47	0.00	2.32
0.5	1.00	9984.57	9497.80	59.01	9995.92	9497.80	61.49
0.5	0.75	9989.91	9622.59	36.88	1.72	9622.59	39.37
0.5	0.50	9994.62	9747.98	18.36	5.99	9747.98	21.00
0.5	0.25	9998.04	9874.72	5.24	9.58	9874.72	8.06
0.5	0.00	0.00	0.00	0.00	11.47	0.00	2.32
1	1.00	9975.69	9505.51	98.75	9987.06	9505.51	101.26
1	0.75	9984.28	9626.65	62.27	9995.75	9626.65	64.90
1	0.50	9991.78	9749.56	31.18	3.26	9749.56	33.81
1	0.25	9997.20	9874.84	8.96	8.79	9874.84	11.72
1	0.00	0.00	0.00	0.00	11.47	0.00	2.32
1.5	1.00	9968.37	9515.62	132.18	9979.97	9515.62	134.54
1.5	0.75	9979.51	9632.31	83.78	9991.21	9632.31	86.36
1.5	0.50	9989.41	9751.62	42.13	0.92	9751.62	44.83
1.5	0.25	9996.55	9875.18	12.11	8.15	9875.18	14.75
1.5	0.00	0.00	0.00	0.00	11.47	0.00	2.32

Table 28: Original Data (90 deg)

Tip Load	Radial Station	Deflection Data					
		Space-Fixed Axes (left side)			Space-Fixed Axes (right side)		
P, lb	r/R, N, D	X, mm	Y, mm	Z, mm	X, mm	Y, mm	Z, mm
0	1.00	8.93	506.42	9989.18	20.32	505.94	9989.48
0	0.75	6.40	380.50	9994.09	18.23	380.34	9994.05
0	0.50	4.22	253.83	9997.31	15.87	253.43	9997.29
0	0.25	2.27	127.08	9999.24	14.02	127.08	9999.02
0	0.00	0.00	0.00	0.00	11.82	0.00	9999.66
0.5	1.00	8.64	505.87	32.76	20.03	505.32	33.07
0.5	0.75	6.98	379.92	22.03	18.61	380.04	21.99
0.5	0.50	4.22	253.83	11.30	16.70	253.43	11.42
0.5	0.25	2.27	127.08	3.28	14.02	127.08	3.05
0.5	0.00	0.00	0.00	0.00	11.82	0.00	9999.66
1	1.00	9.38	499.91	78.45	20.77	500.52	76.28
1	0.75	7.31	376.94	49.44	19.05	376.96	50.39
1	0.50	4.66	252.66	24.89	16.70	252.45	24.75
1	0.25	2.27	127.08	7.47	14.02	127.08	7.18
1	0.00	0.00	0.00	0.00	11.82	0.00	9999.66
1.5	1.00	9.94	491.85	116.36	21.33	491.85	117.23
1.5	0.75	7.66	372.08	75.50	19.52	372.08	75.73
1.5	0.50	5.72	250.92	38.82	16.70	250.92	38.71
1.5	0.25	2.27	127.08	10.94	14.02	127.08	10.85
1.5	0.00	0.00	0.00	0.00	11.82	0.00	9999.66

Table 29: Original Data (-90 deg)

Tip Load	Radial Station	Deflection Data					
		Space-Fixed Axes (left side)			Space-Fixed Axes (right side)		
P, lb	r/R, N, D	X, mm	Y, mm	Z, mm	X, mm	Y, mm	Z, mm
0	1.00	9999.60	9494.11	18.92	11.28	9494.11	18.46
0	0.75	9999.76	9620.88	11.33	11.61	9620.88	11.13
0	0.50	9999.71	9747.87	5.60	11.61	9747.87	5.29
0	0.25	9999.71	9874.98	1.66	11.78	9874.98	1.51
0	0.00	0.00	0.00	0.00	11.78	0.00	9999.98
0.5	1.00	0.02	9498.23	61.28	11.84	9498.23	60.88
0.5	0.75	0.02	9622.97	38.37	11.78	9622.97	38.06
0.5	0.50	9999.80	9748.43	19.04	11.60	9748.43	18.87
0.5	0.25	9999.80	9875.01	5.55	11.68	9875.01	5.43
0.5	0.00	0.00	0.00	0.00	11.78	0.00	9999.98
1	1.00	0.17	9506.75	103.89	12.27	9506.75	103.31
1	0.75	9999.80	9627.38	65.71	11.78	9627.38	65.38
1	0.50	9999.80	9750.13	32.91	11.78	9750.13	32.61
1	0.25	9999.80	9875.13	9.55	11.68	9875.13	9.43
1	0.00	0.00	0.00	0.00	11.78	0.00	9999.98
1.5	1.00	9999.72	9875.66	12.88	11.68	9875.66	12.71
1.5	0.75	9999.96	9752.17	44.69	11.71	9752.17	44.50
1.5	0.50	0.11	9633.24	88.78	12.16	9633.24	88.56
1.5	0.25	1.18	9517.01	139.45	12.56	9517.01	138.97
1.5	0.00	0.00	0.00	0.00	11.78	0.00	9999.98

Table 30: Original Data (180 deg)

Tip Load	Radial Station	Deflection			Angle
		Space-Fixed Axes			(arctan)
P, lb	r/R, N, D	X, mm	Y, mm	Z, mm	Degrees
0	1.00	9,984.42	507.95	2.950	0.000
0	0.75	9,992.18	380.31	1.450	0.000
0	0.50	9,996.39	253.50	1.700	0.000
0	0.25	9,999.09	126.70	0.760	0.000
0	0.00	0.00	0.00	0.000	0.000
3	1.00	9,990.70	507.67	20.350	0.000
3	0.75	9,995.67	379.00	13.500	0.000
3	0.50	9,998.25	253.21	7.280	0.000
3	0.25	9,999.52	126.12	2.660	0.000
3	0.00	0.00	0.00	0.000	0.000

Appendix C: Princeton Beam Data

All recorded data from Beam #2 of the Princeton Beam Experiments is reproduced here, in English units. The experimental data was compared to the current data in Appendix A to determine its general viability, but it is recorded here in its original state. In this case, hyphens represent zero values.

Table 31: Princeton data (0 deg)

Tip Load	Radial Station	Deflection		Angle
		Space-Fixed Axes		use arc-tan
P, lb	r/R, N, D	X, inches	Z, Inches	Degrees
0	1.00	-	-	-
0	0.75	-	-	-
0	0.50	-	-	-
0	0.25	-	-	-
1	1.00	-	0.211	-
1	0.75	-	0.131	-
1	0.50	-	0.069	-
1	0.25	-	0.023	-
2	1.00	-	0.418	-
2	0.75	-	0.265	-
2	0.50	-	0.135	-
2	0.25	-	0.044	-
3	1.00	-	0.631	-
3	0.75	-	0.403	-
3	0.50	-	0.207	-
3	0.25	-	0.060	-
4	1.00	-	0.841	-
4	0.75	-	0.541	-
4	0.50	-	0.284	-
4	0.25	-	0.089	-

Table 32: Princeton data (15 deg)

Tip Load	Radial Station	Deflection		Angle
		Space-Fixed Axes		use arc-tan
P, lb	r/R, N, D	X, inches	Z, Inches	Degrees
0	1.00	-	-	-
0	0.75	-	-	-
0	0.50	-	-	-
0	0.25	-	-	-
1	1.00	0.71	0.400	0.1094
1	0.75	0.46	0.252	0.8451
1	0.50	0.21	0.131	0.5341
1	0.25	0.09	0.039	0.0780
2	1.00	1.50	0.817	1.6410
2	0.75	0.95	0.523	1.6204
2	0.50	0.45	0.250	0.9679
2	0.25	0.18	0.076	0.7611
3	1.00	2.24	1.259	2.3908
3	0.75	1.42	0.796	2.2948
3	0.50	0.68	0.394	2.0569
3	0.25	0.27	0.113	1.1859
4	1.00	3.13	1.754	3.9940
4	0.75	1.93	1.102	4.1172
4	0.50	0.95	0.546	3.7667
4	0.25	0.31	0.152	2.4734

Table 33: Princeton data (-15 deg)

Tip Load	Radial Station	Deflection		Angle
		Space-Fixed Axes		use arc-tan
P, lb	r/R, N, D	X, inches	Z, Inches	Degrees
0	1.00	-	-	-
0	0.75	-	-	-
0	0.50	-	-	-
0	0.25	-	-	-
1	1.00	-0.72	0.406	-0.0024
1	0.75	-0.49	0.263	-0.0050
1	0.50	-0.20	0.131	-0.0074
1	0.25	-0.05	0.041	-2.2666
2	1.00	-1.47	0.837	-1.1445
2	0.75	-0.93	0.535	-0.3197
2	0.50	-0.41	0.266	-0.6912
2	0.25	-0.12	0.077	-0.2171
3	1.00	-2.30	1.289	-2.1968
3	0.75	-1.45	0.825	-1.8252
3	0.50	-0.69	0.410	-1.6144
3	0.25	-0.15	0.121	-1.1421
4	1.00	-3.11	1.796	-3.4526
4	0.75	-2.01	1.141	-3.5529
4	0.50	-1.01	0.563	-2.9438
4	0.25	-0.22	0.164	-2.0559

Table 34: Princeton data (30 deg)

Tip Load	Radial Station	Deflection		Angle
		Space-Fixed Axes		use arc-tan
P, lb	r/R, N, D	X, inches	Z, Inches	Degrees
0	1.00	-	-	-
0	0.75	-	-	-
0	0.50	-	-	-
0	0.25	-	-	-
1	1.00	1.22	0.936	0.4028
1	0.75	0.75	0.594	0.1875
1	0.50	0.36	0.293	-0.0163
1	0.25	0.12	0.084	-0.1227
2	1.00	2.43	1.893	1.6828
2	0.75	1.58	1.198	1.0285
2	0.50	0.72	0.596	0.7459
2	0.25	0.23	0.168	0.5946
3	1.00	3.68	2.862	3.6308
3	0.75	2.31	1.814	3.1476
3	0.50	1.13	0.893	3.0160
3	0.25	0.38	0.248	2.1725
4	1.00	4.73	3.853	5.8569
4	0.75	3.01	2.443	5.8524
4	0.50	1.50	1.207	5.0895
4	0.25	0.43	0.331	3.7772

Table 35: Princeton data (-30 deg)

Tip Load	Radial Station	Deflection		Angle
		Space-Fixed Axes		use arc-tan
P, lb	r/R, N, D	X, inches	Z, Inches	Degrees
0	1.00	-	-	-
0	0.75	-	-	-
0	0.50	-	-	-
0	0.25	-	-	-
1	1.00	-1.26	0.951	-0.2509
1	0.75	-0.81	0.608	-0.0670
1	0.50	-0.40	0.310	-0.1883
1	0.25	-0.13	0.083	-0.0718
2	1.00	-2.48	1.909	-1.2960
2	0.75	-1.59	1.213	-1.4850
2	0.50	-0.77	0.609	-1.2823
2	0.25	-0.23	0.168	-0.2310
3	1.00	-3.64	2.902	-3.2471
3	0.75	-2.31	1.837	-3.2691
3	0.50	-1.12	0.921	-3.1822
3	0.25	-0.32	0.252	-1.6200
4	1.00	-4.71	3.900	-5.6334
4	0.75	-2.98	2.480	-5.5118
4	0.50	-1.51	1.229	-5.1528
4	0.25	-0.41	0.341	-3.6230

Table 36: Princeton data (45 deg)

Tip Load	Radial Station	Deflection		Angle
		Space-Fixed Axes		use arc-tan
P, lb	r/R, N, D	X, inches	Z, Inches	Degrees
0	1.00	-	-	-
0	0.75	-	-	-
0	0.50	-	-	-
0	0.25	-	-	-
1	1.00	1.42	1.652	0.6378
1	0.75	0.90	1.049	0.8850
1	0.50	0.48	0.520	0.7558
1	0.25	0.12	0.143	0.6675
2	1.00	2.72	3.234	1.8583
2	0.75	1.73	2.068	1.6232
2	0.50	0.88	1.027	1.5632
2	0.25	0.22	0.288	1.1775
3	1.00	3.89	4.731	3.7187
3	0.75	2.50	3.024	3.5301
3	0.50	1.28	1.505	3.1347
3	0.25	0.33	0.427	2.4877

Table 37: Princeton data (-45 deg)

Tip Load	Radial Station	Deflection		Angle
		Space-Fixed Axes		use arc-tan
P, lb	r/R, N, D	X, inches	Z, Inches	Degrees
0	1.00	-	-	-
0	0.75	-	-	-
0	0.50	-	-	-
0	0.25	-	-	-
1	1.00	-1.32	1.661	-0.3658
1	0.75	-0.91	1.058	-0.8041
1	0.50	-0.43	0.527	-0.4124
1	0.25	-0.11	0.143	-0.5666
2	1.00	-2.80	3.270	-1.8583
2	0.75	-1.77	2.082	-2.0698
2	0.50	-0.89	1.039	-1.5805
2	0.25	-0.25	0.286	-1.2095
3	1.00	-3.88	4.773	-3.6141
3	0.75	-2.49	3.043	-3.8712
3	0.50	-1.24	1.520	-3.2489
3	0.25	-0.39	0.427	-2.4178

Table 38: Princeton data (60 deg)

Tip Load	Radial Station	Deflection		Angle
		Space-Fixed Axes		use arc-tan
P, lb	r/R, N, D	X, inches	Z, Inches	Degrees
0	1.00	-	-	-
0	0.75	-	-	-
0	0.50	-	-	-
0	0.25	-	-	-
0.5	1.00	0.60	1.201	0.1866
0.5	0.75	0.38	0.764	0.2057
0.5	0.50	0.18	0.382	0.2295
0.5	0.25	0.09	0.103	0.1221
1	1.00	1.20	2.356	0.4267
1	0.75	0.74	1.499	0.3740
1	0.50	0.38	0.752	0.3616
1	0.25	0.13	0.210	0.1259
1.5	1.00	1.77	3.474	0.8956
1.5	0.75	1.15	2.210	0.9621
1.5	0.50	0.57	1.104	0.7441
1.5	0.25	0.18	0.307	0.5094
2	1.00	2.30	4.516	1.4864
2	0.75	1.49	2.884	1.3614
2	0.50	0.72	1.441	0.9114
2	0.25	0.22	0.410	0.6956

Table 39: Princeton data (-60 deg)

Tip Load	Radial Station	Deflection		Angle
		Space-Fixed Axes		use arc-tan
P, lb	r/R, N, D	X, inches	Z, Inches	Degrees
0	1.00	-	-	-
0	0.75	-	-	-
0	0.50	-	-	-
0	0.25	-	-	-
0.5	1.00	-0.66	1.203	-0.1241
0.5	0.75	-0.43	0.757	-0.1390
0.5	0.50	-0.19	0.382	-0.1159
0.5	0.25	-0.01	0.109	-0.0829
1	1.00	-1.18	2.358	-0.2512
1	0.75	-0.80	1.495	-0.4888
1	0.50	-0.36	0.745	-0.2572
1	0.25	-0.04	0.209	-0.1327
1.5	1.00	-1.79	3.479	-0.6188
1.5	0.75	-1.18	2.208	-0.7756
1.5	0.50	-0.55	1.101	-0.9466
1.5	0.25	-0.11	0.311	-0.4327
2	1.00	-2.28	4.526	-1.3466
2	0.75	-1.50	2.876	-1.6671
2	0.50	-0.70	1.436	-1.5114
2	0.25	-0.23	0.407	-1.0508

Table 40: Princeton data (75 deg)

Tip Load	Radial Station	Deflection		Angle
		Space-Fixed Axes		use arc-tan
P, lb	r/R, N, D	X, inches	Z, Inches	Degrees
0	1.00	-	-	-
0	0.75	-	-	-
0	0.50	-	-	-
0	0.25	-	-	-
0.5	1.00	0.35	1.454	-0.0005
0.5	0.75	0.23	0.927	0.0495
0.5	0.50	0.12	0.451	-0.0092
0.5	0.25	0.01	0.132	0.0460
1	1.00	0.71	2.846	0.2586
1	0.75	0.47	1.817	0.1171
1	0.50	0.20	0.901	0.2213
1	0.25	0.05	0.257	0.2180
1.5	1.00	1.03	4.190	0.5293
1.5	0.75	0.67	2.668	0.5076
1.5	0.50	0.31	1.340	0.4430
1.5	0.25	0.06	0.382	0.3287

Table 41: Princeton data (-75 deg)

Tip Load	Radial Station	Deflection		Angle
		Space-Fixed Axes		use arc-tan
P, lb	r/R, N, D	X, inches	Z, Inches	Degrees
0	1.00	-	-	-
0	0.75	-	-	-
0	0.50	-	-	-
0	0.25	-	-	-
0.5	1.00	-0.40	1.454	-0.0895
0.5	0.75	-0.23	0.927	-0.1598
0.5	0.50	-0.12	0.458	-0.0953
0.5	0.25	-0.03	0.130	0.0449
1	1.00	-0.60	2.883	-0.1913
1	0.75	-0.45	1.831	-0.3479
1	0.50	-0.21	0.908	-0.3467
1	0.25	-0.05	0.266	0.0692
1.5	1.00	-1.02	4.204	-0.5117
1.5	0.75	-0.67	2.676	-0.4276
1.5	0.50	-0.33	1.339	-0.3634
1.5	0.25	-0.06	0.380	-0.1962

Table 42: Princeton data (90 deg)

Tip Load	Radial Station	Deflection		Angle
		Space-Fixed Axes		use arc-tan
P, lb	r/R, N, D	X, inches	Z, Inches	Degrees
0	1.00	-	-	-
0	0.75	-	-	-
0	0.50	-	-	-
0	0.25	-	-	-
0.5	1.00	-	1.560	-
0.5	0.75	-	0.984	-
0.5	0.50	-	0.497	-
0.5	0.25	-	0.136	-
1	1.00	-	3.048	-
1	0.75	-	1.938	-
1	0.50	-	0.973	-
1	0.25	-	0.275	-
1.5	1.00	-	4.453	-
1.5	0.75	-	2.841	-
1.5	0.50	-	1.428	-
1.5	0.25	-	0.404	-

Table 43: Princeton data (-90 deg)

Tip Load	Radial Station	Deflection		Angle
		Space-Fixed Axes		use arc-tan
P, lb	r/R, N, D	X, inches	Z, Inches	Degrees
0	1.00	-	-	-
0	0.75	-	-	-
0	0.50	-	-	-
0	0.25	-	-	-
0.5	1.00	-	1.569	-
0.5	0.75	-	0.996	-
0.5	0.50	-	0.494	-
0.5	0.25	-	0.137	-
1	1.00	-	3.065	-
1	0.75	-	1.954	-
1	0.50	-	0.969	-
1	0.25	-	0.277	-
1.5	1.00	-	4.449	-
1.5	0.75	-	2.838	-
1.5	0.50	-	1.416	-
1.5	0.25	-	0.400	-

Table 44: Princeton data (180 deg)

Tip Load	Radial Station	Deflection		Angle
		Space-Fixed Axes		use arc-tan
P, lb	r/R, N, D	X, inches	Z, Inches	Degrees
0	1.00	-	-	-
0	0.75	-	-	-
0	0.50	-	-	-
0	0.25	-	-	-
3	1.00	-	0.646	-
3	0.75	-	0.451	-
3	0.50	-	0.206	-
3	0.25	-	0.056	-

6. Works Cited

Dowell, E. H., and J. J. Traybar. An Experimental Study of the Nonlinear Stiffness of a Rotor Blade Undergoing Flap, Lag, and Twist Deformations. U.S. Army Air Mobility Research Development Laboratory. Moffett Field: Ames Research Center, 1975.

Hinnant, Howard E., and Dewey H. Hodges. Nonlinear Analysis of a Cantilever Beam. Ames Research Center. Moffett Field: Georgia Institute of Technology, 1988.

Hodges, Dewey H., A. S. Hopkins, Donald L. Kunz, and Howard E. Hinnant. Introduction to GRASP-General Rotorcraft Aeromechanical Stability Program-a Modern Approach to Rotorcraft Modeling. U.S. Army Aviation Research and Technology Activity. Alexandria: The American Helicopter Society, 1987.

Hodges, Dewey H. Rotor Blade and Beam Theory: Past, Present, and Future. Georgia Institute of Technology. Boca Raton: The Daniel Guggenheim School of Aerospace Engineering, 2005.

Hopkins, A. S., and Robert A. Ormiston. An Examination of Selected Problems in Rotor Blade Structural Mechanics and Dynamics. US Army Aviation and Missile Command. Moffett Field: NASA Ames Research Center, 2003.

REPORT DOCUMENTATION PAGE

Form Approved
OMB No. 074-0188

1. REPORT DATE *(DD-MM-YYYY)*	**2. REPORT TYPE**	**3. DATES COVERED** *(From – To)*
05-06-2006	**Master's Thesis**	13JUN06 – 13JUN06

4. TITLE AND SUBTITLE

An Analysis of Nonlinear Elastic Deformations for a Homogeneous Beam at Varying Tip Loads and Pitch Angles

5a. CONTRACT NUMBER

5b. GRANT NUMBER

5c. PROGRAM ELEMENT NUMBER

6. AUTHOR(S)

McGraw, Robert J. ENS/USN

5d. PROJECT NUMBER
N/A

5e. TASK NUMBER

5f. WORK UNIT NUMBER

7. PERFORMING ORGANIZATION NAMES(S) AND ADDRESS(S)
Air Force Institute of Technology
Graduate School of Engineering and Management (AFIT/EN)
2950 Hobson Way
WPAFB OH 45433-7765

8. PERFORMING ORGANIZATION REPORT NUMBER

AFIT/GAE/ENY/06-J09

9. SPONSORING/MONITORING AGENCY NAME(S) AND ADDRESS(ES)

Dr. Robert A. Ormiston
U.S. Army Aerodynamics Directorate
NASA Ames Research Center, MS 215-1
Moffett Field, CA 94035-100

10. SPONSOR/MONITOR'S ACRONYM(S)

11. SPONSOR/MONITOR'S REPORT NUMBER(S)

12. DISTRIBUTION/AVAILABILITY STATEMENT

APPROVED FOR PUBLIC RELEASE; DISTRIBUTION UNLIMITED.

13. SUPPLEMENTARY NOTES

14. ABSTRACT

The Princeton beam experiments of 1975 were performed in hopes of producing viable data for beam nonlinear elastic deformation models in hopes of improving helicopter main beam designs. The recorded data, specifically for homogeneous beams of 7075 aluminum, have been referenced as a baseline for the past thirty years to validate numerous computer models and theories in an effort to build beams capable of withstanding aeroelastic, static, and dynamic loading.

The purpose of this study is to improve upon the data recorded in 1975 using newer technologies including a laser distance meter, digital inclinometer, and three-dimensional traverse to test X-axis, Y-axis, Z-axis and angular displacements for varying tip loads and pitch angles.

Initial beam deformations due to machining stresses were included in the testing, and the beam was analyzed at tip loads between zero and four pounds for positive and negative pitch angles in fifteen-degree increments from zero to ninety degrees. The results were analyzed in numerous comparisons between the different tip loads and pitch angles, and the overall results were compared with Princeton beam data to ensure their validity.

The experimental results showed an improvement in terms of precision as well as a relatively close correlation with Princeton beam data. There were some displacement discrepancies, but such differences can be examined in the future. The results can be used for beam vibrational mode and frequency testing as the beam's geometry can be reproduced graphically and computer model verifications, allowing for more precise computer models for homogeneous nonlinear beam displacements.

15. SUBJECT TERMS: beam deflection, nonlinear deflection, beam displacement, rotor blade analysis, Princeton beam experiment, beam static and dynamic loading

16. SECURITY CLASSIFICATION OF:			**17. LIMITATION OF ABSTRACT**	**18. NUMBER OF PAGES**	**19a. NAME OF RESPONSIBLE PERSON**
REPORT	**ABSTRACT**	**c. THIS PAGE**			Dr. Donald Kunz
U	**U**	**U**	**UU**	106	**19b. TELEPHONE NUMBER** *(Include area code)* (937) 785-3636, ext 4548; e-mail: donald.kunz@afit.edu

Standard Form 298 (Rev: 8-98)
Prescribed by ANSI Std. Z39-18